climate

MDPI

Article

The Performance of a High-Resolution WRF Modelling System in the Simulation of Severe Tropical Cyclones over the Bay of Bengal Using the IMDAA Regional Reanalysis Dataset

Thatiparthi Koteshwaramma [1], Kuvar Satya Singh [2,*] and Sridhara Nayak [3,*]

[1] Department of Mathematics, School of Advanced Sciences (SAS), Vellore Institute of Technology, Vellore 632014, Tamil Nadu, India; koteshwaramma.t2021@vitstudent.ac.in
[2] Centre for Disaster Mitigation and Management (CDMM), Vellore Institute of Technology, Vellore 632014, Tamil Nadu, India
[3] Research and Development Center, Japan Meteorological Corporation Limited, Osaka 530-0011, Japan
* Correspondence: kuvarsatya.singh@vit.ac.in (K.S.S.); nayak.sridhara@n-kishou.co.jp (S.N.)

Abstract: Extremely severe cyclonic storms over the North Indian Ocean increased by approximately 10% during the past 30 years. The climatological characteristics of tropical cyclones for 38 years were assessed over the Bay of Bengal (BoB). A total of 24 ESCSs formed over the BoB, having their genesis in the southeast BoB, and the intensity and duration of these storms have increased in recent times. The Advanced Research version of the Weather Research and Forecasting (ARW) model is utilized to simulate the five extremely severe cyclonic storms (ESCSs) over the BoB during the past two decades using the Indian Monsoon Data Assimilation and Analysis (IMDAA) data. The initial and lateral boundary conditions are derived from the IMDAA datasets with a horizontal resolution of 0.12° × 0.12°. Five ESCSs from the past two decades were considered: Sidr 2007, Phailin 2013, Hudhud 2014, Fani 2019, and Amphan 2020. The model was integrated up to 96 h using double-nested domains of 12 km and 4 km. Model performance was evaluated using the 4 km results, compared with the available observational datasets, including the best-fit data from the India Meteorological Department (IMD), the Tropical Rainfall Measuring Mission (TRMM) satellite, and the Doppler Weather Radar (DWR). The results indicated that IMDAA provided accurate forecasts for Fani, Hudhud, and Phailin regarding the track, intensity, and mean sea level pressure, aligning well with the IMD observational datasets. Statistical evaluation was performed to estimate the model skills using Mean Absolute Error (MAE), the Root Mean Square Error (RMSE), the Probability of Detection (POD), the Brier Score, and the Critical Successive Index (CSI). The calculated mean absolute maximum sustained wind speed errors ranged from 8.4 m/s to 10.6 m/s from day 1 to day 4, while mean track errors ranged from 100 km to 496 km for a day. The results highlighted the prediction of rainfall, maximum reflectivity, and the associated structure of the storms. The predicted 24 h accumulated rainfall is well captured by the model with a high POD (96% for the range of 35.6–64.4 mm/day) and a good correlation (65–97%) for the majority of storms. Similarly, the Brier Score showed a value of 0.01, indicating the high performance of the model forecast for maximum surface winds. The Critical Successive Index was 0.6, indicating the moderate model performance in the prediction of tracks. It is evident from the statistical analysis that the performance of the model is good in forecasting storm structure, intensity and rainfall. However, the IMDAA data have certain limitations in predicting the tracks due to inadequate representation of the large-scale circulations, necessitating improvement.

Keywords: IMDAA; ESCS; WRF; Bay of Bengal; reanalysis

Academic Editor: Helena A. Flocas

Received: 19 November 2024
Revised: 28 December 2024
Accepted: 7 January 2025
Published: 13 January 2025

Citation: Koteshwaramma, T.; Singh, K.S.; Nayak, S. The Performance of a High-Resolution WRF Modelling System in the Simulation of Severe Tropical Cyclones over the Bay of Bengal Using the IMDAA Regional Reanalysis Dataset. *Climate* **2025**, *13*, 17. https://doi.org/10.3390/cli13010017

1. Introduction

Over the North Indian Ocean (NIO), the intensity and frequency of tropical cyclones (TCs) are increasing [1–6], and the population density near the coastal belts has also increased [7,8]. Hence, the risk associated with landfalling TCs over coastal regions in terms of coastal vulnerability also increases [9]. Many studies suggest that the Indian subcontinent is highly vulnerable to TCs compared to other regions, and the forecast accuracy of TCs is lower compared to those in the North Atlantic and Pacific Oceans [10,11]. Extremely severe cyclonic storms over the North Indian Ocean increased by approximately 10% during the past 30 years (1996–2021) compared to the period 1972–1995 [6]. Observations also revealed an increasing trend in the duration of the ESCS, stage, and wind speed over the NIO [5]. The present warming climate has significant impacts on the formation of tropical cyclones over the Bay of Bengal (BOB) region, affecting densely populated coastal cities such as Chennai, Visakhapatnam, Bhubaneswar, and Kolkata, which are close to the BoB [12]. As a result, the projected global warming conditions and anticipated climate changes in the near future are expected to lead to the intensification of extremely severe cyclonic storms (ESCSs) under the tropical cyclone category [13–16]. Several researchers have indicated that forecasting extremely severe cyclonic storms (ESCSs) is essential to provide early warning forecasts of storm surges and coastal inundation, evacuate coastal communities, and ensure implementation of the preparedness strategies to save lives and property from climate change impacts [17]. Therefore, there is a need to improve the forecasting skill of intense TCs over the NIO. In the last two decades, the forecast accuracy of TCs has increased by using high-resolution regional and global numerical weather prediction models [18–22] and proper representation of physical parameterization schemes [23–28]. Additionally, TC forecast accuracy has been enhanced by using advanced data assimilation techniques such as 3D/4D variational techniques as well as hybrid and ensemble methods [5,29–43]. Previous studies have indicated that although track forecasts have improved, intensity forecasts are still limited. It is essential to test the performance of a modeling system in forecasting TCs for a period of 96 h, including track, intensity, and landfall by comparing several cases developed over the Bay of Bengal region in a high-resolution modeling system. It has been highlighted that increasing the horizontal resolution in the HWRF model has a larger impact on predicting intense cyclones than low-intensity cyclones [44]. Additionally, increased horizontal resolution provides a better forecast of warm core structures and secondary circulations [45,46]. Several studies have also documented that improved model horizontal resolutions positively impact the forecast of track and intensity [47,48]. Reanalysis datasets are provided by various meteorological centers based on numerical weather prediction systems, with significant improvements in models and data assimilation schemes [49]. These datasets represent various advancements in the prediction of TC characteristics. The European Centre for Medium-Range Weather Forecasts (ECMWF) fifth-generation global atmospheric reanalysis (ERA5), with a horizontal resolution of 31 km, resolves higher radial pressure gradients and stronger TC winds for smaller TC sizes. However, it underestimates these features for larger TC sizes. Similarly, the National Centres for Environmental Prediction (NCEP) Climate Forecast System Reanalysis (CFSR) and the ECMWF Interim Reanalysis (ERAI) datasets overestimate stronger winds for smaller TC sizes and underestimate them for larger sizes. Lee et al. (2023) reported that reanalysis datasets, such as the NCAR 20th-Century Reanalysis Version 3 dataset (20CRv3), the Japanese 55-Year Reanalysis dataset (JRA55), the National Centers for Environmental Prediction and National Center for Atmospheric Research (NCEP/NCAR) Reanalysis dataset (NCAR), the European Centre for Medium-Range Weather Forecasts Reanalysis Interim dataset (ERAI), the Fifth Generation of Atmospheric Reanalysis dataset (ERA5), and the 20th-Century Reanalysis of the European Centre for Medium-Range Weather Forecasts

(ERA20C), have different assimilation methods, model resolutions, and TC treatments, leading to variations in large-scale flow, frequency, accurate location, sea level pressure, and wind distribution around TCs [50]. In addition, they reported that reanalysis datasets failed to capture the low TC genesis years between 1998 and 2014. Ref. [51] analyzed the regional IMDAA reanalysis dataset over the North Indian Ocean (NIO) considering 197 storms during the period 1979–2018, and they reported that TC tracks are well represented, but the intensity and associated properties of TCs are not well captured. Ref. [52] analyzed ERAI, the Global Forecast System (GFS) analysis, JRA55, the Modern-Era Retrospective Analysis for Research and Applications Version 2 (MERRA2), NCEP Climate Forecast System Reanalysis (CFSR), and ERA5 for the representation of track, intensity, and structure of 28 TCs over the NIO. They reported that the GFS dataset provided a better representation of TC structures compared to other datasets but showed overprediction and early intensification for high-intensity category TCs.

From the above, it is clear that using a high-resolution modeling system provides a better forecast of the track, structure, and intensity of TCs. However, in most of these studies, the initial conditions and boundary conditions of tropical storms are derived mainly from the NCEP Final Analysis (FNL; $1.0^\circ \times 1.0^\circ$ resolution), Global Forecast System (GFS; $0.5^\circ \times 0.5^\circ$ resolution), and ECMWF Reanalysis Interim/ERA5 ($0.25^\circ \times 0.25^\circ$ resolution) datasets. In recent days, a very high-resolution regional reanalysis dataset, namely Indian Monsoon Data Assimilation and Analysis (IMDAA), is available, which is used for the prediction of monsoon and precipitation intensity over the Indian subcontinent. The IMDAA data, prepared using the 4D-Var data assimilation method, integrates surface and upper-air observations, satellite, and radar data with a horizontal resolution of 12 km at 6 h intervals. This emphasized that the significant role of horizontal resolution during data assimilation is to improve TC intensity forecasts [44]. A higher horizontal resolution enhances the accuracy of initial conditions by capturing small-scale features of the cyclone, such as the eyewall and inner-core dynamics. This improvement leads to better representation of updrafts and condensation processes, resulting in stronger adiabatic heating in the cyclone's eyewall and an increase in intensity. The enhanced resolution ensures better initialization of key cyclone characteristics, such as the position and strength of the low-pressure vortex, which are critical for accurate forecasts. It is necessary to test the performance of the high-resolution weather forecasting model using the regional dataset in the forecast of intense tropical cyclones over the Bay of Bengal region.

In addition, the literature highlights a significant increase in approximately 26% in ESCSs over the North Indian Ocean in the past 30 years. Also, recent observations indicate a rising trend in the duration of the ESCS stage and wind speed. The cumulative effects of these ESCSs contribute to elevated storm surge heights and increased inundation along the coast, resulting in devastating damage to lives and property in coastal regions. In the future, the anticipated increase in global warming and human-induced climate change may lead to the formation of numerous ESCSs over the BoB and globally. Identifying these research gaps has motivated the development of a customized high-resolution WRF modeling system to forecast the ESCSs over the BoB.

A customized high-resolution ARW modeling system utilizing the high-resolution IMDAA reanalysis dataset will provide a more accurate forecast for various TCs, instilling confidence in the model's predictability. Hence, the performance of the IMDAA datasets in a high-resolution ARW model was tested to forecast five different land-falling TCs over the region under varying environmental conditions. The purpose of this study was to evaluate the model's efficiency in simulating five extremely severe cyclonic storms (ESCSs; wind speed exceeding 90 knots) using the IMDAA datasets under diverse environmental

conditions. These storms developed over the Bay of Bengal region and made landfall in different parts of the Indian subcontinent.

The structure is organized as follows: In Section 2, the methodology, this study's datasets and the numerical experiments are detailed. In Section 3, the results from the nested domain of 4 km are presented and discussed. The last section provides a discussion of this study's results and conclusions.

2. Methodology and Data

This study utilized the Advanced Research version of the Weather Research and Forecasting (ARW) model, specifically ARW (V 4.2). This model consists of features like non-hydrostatic, terrain-following sigma coordinates as vertical coordinates, a time integration scheme using the Runge-Kutta 3rd order, and various choices for dynamics, numeric, and physics components [53]. The ARW model is configured with two nesting domains: an outer domain with a resolution of 12 km (355 × 430 grid points, covering approximately 65° E–110° E and 10° S–40° N) and an inner domain with a resolution of approximately 4 km (523 × 682 grid points, covering approximately 78.42° E–100.06° E and 0.11° N–27.07° N). This setup encompasses the Bay of Bengal and its regions (Figure 1). This improves the representation of the topographic features of the terrain and other atmospheric processes [54–58]. The model has 51 unequal vertical levels with a model top at 10 hPa. Physical settings for this study were selected from previous modeling studies over the Bay of Bengal region, demonstrating improved forecasts of tropical cyclones [24,25,31,59–61]. These selected physics included microphysics, cumulus, planetary boundary layer, long/short-wave radiations, and land surface models. Table 1 provides details of the selected model configuration used in this study.

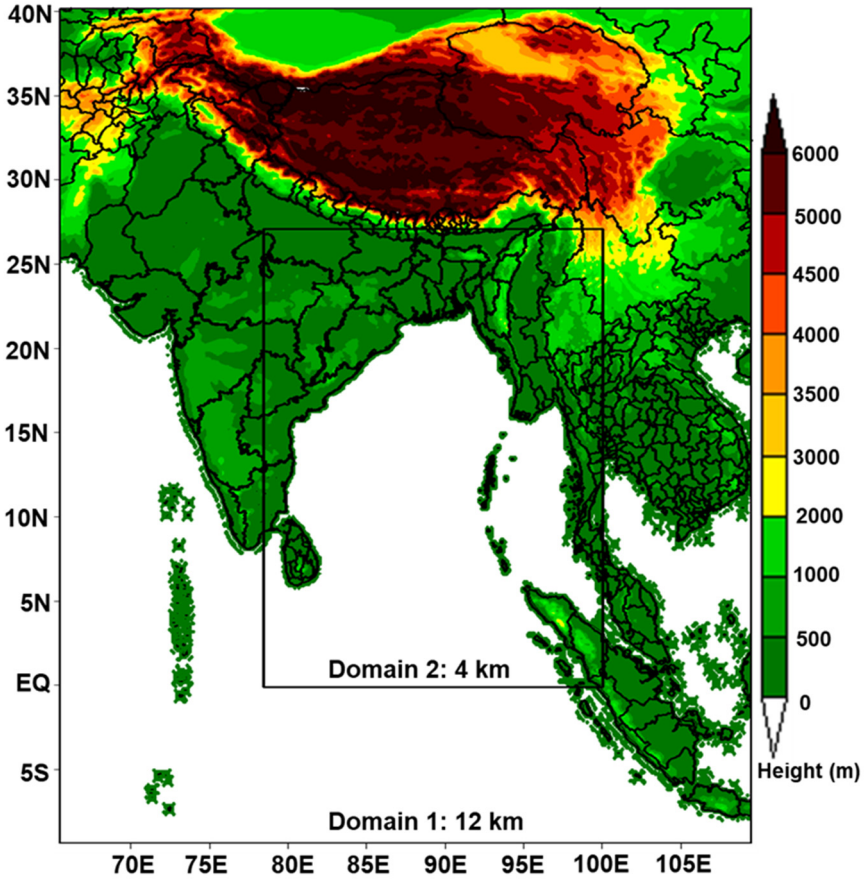

Figure 1. Study area map showing topography and the configured domains. The domains have horizontal resolutions of 12 km and 4 km, respectively.

Table 1. Model configuration used in this study for the 5 ESCS simulations.

Dynamical Core	**ARW, Non-Hydrostatic**
Horizontal grid distance	Domain 1: 12 km Domain 2: 4 km
Initial and lateral boundary conditions	IMDAA reanalysis
Boundary conditions updated	6 h
Number of vertical levels	51
Integration time step	60 s (D1) and 20 s (D2)
Microphysical scheme	Lin [62,63]
Cumulus parameterization	Kain-Fritsch [64] (D1)
PBL scheme	YSU [65]
Radiation schemes	LW-RRTM [66] and SW-Dudhia [67]
Land surface model	Noah [68]

Table 2 presents information on five extremely severe cyclonic storms (ESCSs) selected for simulations, including details on formation, landfall position, and initialization time. Notably, each experiment had a forecast length of 96 h. The model's initial and lateral boundary conditions for simulating ESCSs over the Bay of Bengal region were derived from the Indian Monsoon Data Assimilation and Analysis reanalysis (IMDAA) of the North Indian Ocean. This reanalysis dataset has a horizontal resolution of $0.12^\circ \times 0.12^\circ$ over the Indian subcontinent [69–71] with 63 vertical levels to reach a height of approximately 40 km, covering the region between 30° to 120° E and 15° S to 45° N over the North Indian Ocean. The Indian Monsoon Data Assimilation and Analysis (IMDAA) system utilizes the Four-Dimensional Variational Data Assimilation (4D-Var) technique. This data assimilation approach employs a minimization approach to generate reanalysis data by incorporating background forecasts and observational data. Considering the associated uncertainties, the method aims to strike a balance between model predictions and available recorded observations. Several experiments were conducted using different configurations, including model resolutions of 15 km and 5 km, as well as 12 km and 4 km resolutions. These experiments involved varying initial conditions, such as 00 UTC and 12 UTC, and change in the reported best physical parameterization schemes over the study region to assess the model forecast sensitivity with the IMDAA regional reanalysis dataset. Finally, the WRF model was integrated with a time step of 60 s for a 12 km resolution in Domain 1 (D1) and 20 s for a 4 km in Domain 2 (D2). The boundary conditions were applied at 6 h intervals using the IMDAA regional reanalysis dataset. To assess the ARW modeling system's capability of using the IMDAA reanalysis datasets as initial and boundary conditions, five extremely severe cyclonic storms (ESCSs)—Sidr 2007, Phailin 2013, Hudhud 2014, Fani 2019, and Amphan 2020—were selected for simulations. These five ESCSs events, selected from the climatological period of 2007–2020 (~14 years), represent the increasing intensity of storms in the region. These events highlight their effects on rising storm surges and coastal flooding. Table 2 provides the initialization times for each cyclone, and the model initialization techniques involve selecting different stages of the formation of a low-pressure system, such as the depression and cyclone stages, by covering a forecast duration of 96 h.

Table 2. Details of extremely severe cyclonic storms considered in this study.

Name of Cyclone	Initialization Stage	Landfall Location	Initialization Time
Amphan (May 2020)	Cyclonic	West Bengal coast, [21.65 N, 88.3 E]	00 UTC on 17 May 2020
Fani (April 2019)	Cyclonic	Puri, Odisha, [19.75 N, 85.7 E]	00 UTC on 29 April 2019
Hudhud (October 2014)	Cyclonic	Vishakhapatnam, AP, [17.7 N, 83.3 E]	00 UTC on 9 October 2014
Phailin (October 2013)	Deep depression	Gopalpur, Odisha, [19.2 N, 84.9 E]	00 UTC on 09 October 2013
Sidr (November 2007)	Deep depression	Bangladesh coast, [21.8 N, 89.8 E]	00 UTC on 12 November 2007

This study presents simulations of cyclone movement, intensity (maximum surface wind and minimum central pressure), 24 h wind speed and direction changes, daily accumulated rainfall, maximum reflectivity, and discussion on derived parameters like time series of warm core structure and frozen hydrometeors for the ESCSs. To validate the rainfall pattern and distribution, the simulated results were compared with IMD-best-fit track, the Doppler weather radar from IMD, and rainfall data from the Tropical Rainfall Measuring Mission (TRMM; daily accumulated precipitation combined microwave-IR (GPM_3IMERGDF v06)), with a spatial resolution of $0.1^\circ \times 0.1^\circ$. Additionally, the model's forecasted warm core structure was compared to AMSU satellite-derived data [72]. The best-track is defined as the track of a cyclone throughout its lifecycle, determined through post-event analysis, providing accurate information about its position, intensity, landfall location, and other characteristics at regular time intervals. This is provided by the India Meteorological Department (IMD), Government of India, at 6-hourly intervals (https://rsmcnewdelhi.imd.gov.in/report.php, accessed on 14 January 2023). This includes data from automatic weather stations, buoy observations, ship observations, satellite data, and radar observations [73,74]. This is used to validate model-simulated tracks, intensity, and landfall locations for five ESCSs over the Bay of Bengal, and to estimate track errors and biases in cyclonic parameters. We made a preliminary assessment of the IMDAA reanalysis dataset with other global reanalysis datasets, such as FNL and ECMWF, to evaluate the strength of the data for storm prediction and details are presented in Table 3.

Table 3. Comparison of IMDAA regional reanalysis data with the ERA-Interim and NCEP FNL global reanalysis datasets for five ESCSs over the Bay of Bengal.

Cyclone	Initial Position Error (km) Compared to IMD Data			Surface Wind Speed (m/s)			Relative Humidity (%)			Vertical Wind Shear (m/s) Between 850 and 200 hPa		
	ERA-Interim	FNL	IMDAA	ERA-Interim	FNL	IMDAA	ERA-Interim	FNL	IMDAA	ERA-Interim	FNL	IMDAA
Amphan	46	44	87	26	24	16	83	83	74	4.8	6.4	3.7
Fani	234	60	35	15	28	24	81	77	79	0.5	2.8	3.9
Hudhud	123	22	47	13	25	18	82	85	88	2.4	3.4	3.1
Phailin	489	89	120	10	16	12	78	84	84	0.77	5.0	2.3
Sidr	78	85	127	12	13	20	74	76	81	0.7	1.5	1.1

Statistical analysis was performed on forecasted cyclonic parameters, including cyclone track errors, maximum surface wind speed, 24 h accumulated rainfall, and landfall locations of ESCSs, using various statistical methods. These methods include track error (TE), the Mean Absolute Error (MAE), the Root Mean Square Error (RMSE), and skill scores such as the

Probability of Detection (POD), the Brier Score (BS), and the Critical Success Index (CSI) to evaluate the performance of the WRF modeling system with the IMDAA dataset.

Track error (TE) was calculated as the difference between the forecasted track and the best-track data from IMD at specific times, with the angular difference converted to distance by multiplying by 111 km (distance of each degree of latitude and longitude). The MAE was estimated from differences in maximum surface wind speeds between forecasted and observational data [75]. The RMSE was calculated to quantify error patterns between the model-forecasted parameters and observations [76].

$$\text{TE (in km)} = \sqrt{(\Delta lat)^2 + (\Delta lon)^2} \times 111 \quad (1)$$

$$\text{MAE} = \frac{\sum |O_i - P_i|}{n} \quad (2)$$

$$\text{RMSE} = \sqrt{\frac{\sum (P_i - O_i)^2}{n}} \quad (3)$$

where n is the total sample size, P_i is the predicted value and O_i is the observed value for the ith sample.

To evaluate the model skill score, the Probability of Detection (POD) was used to compare model-predicted rainfall from IMDAA data with observations from TRMM and 174 automatic weather stations across Odisha during Cyclone Phailin. The analysis focused on rainfall intensities between 64.5 and 115.5 mm/day, calculated using a 2×2 contingency table with values of 1 and 0, indicating "good" and "poor" predictions, respectively [77].

The Brier Score is another skill scoring method used to measure the mean squared error between forecast probability and observed frequency [78]. This is presented as follows:

$$\text{BS} = \frac{1}{N} \sum_{i=1}^{N} (P_i - O_i)^2 \quad (4)$$

where N is the total sample size, P_i is the forecast probability and O_i is the observed frequency for the ith sample. Therefore, a Bias Score (BS) value of 0 represents the closest accuracy. This skill score metric evaluates model performance in forecasting storm intensity.

The Critical Success Index (CSI) is another metric for measuring the accuracy of severe weather predictions, following the procedure outlined by [79]. The CSI value ranges from 0 to 1, where a value of 1 indicates a perfect forecast by the model. This metric is used to evaluate the accuracy of a model forecast for landfall location.

3. Results and Discussions

This section elaborates the climatological changes in the tropical cyclones regarding the genesis, intensity and their trends over the BoB. The role of the IMDAA datasets in forecasting five extremely severe cyclonic storms (ESCSs) that developed over the Bay of Bengal region and made landfall along different parts of the eastern coast of India and Bangladesh is highlighted using WRF model. The results primarily focus on the forecasted track, maximum surface wind (MSW), central sea level pressure (CSLP), storm structure, and rainfall during the 96-h simulation and the warm core structure of the storms.

3.1. Climatological Analysis of Tropical Cyclones over the Bay of Bengal

The climatological analysis of tropical cyclones over the Bay of Bengal (BoB) is shown in Figure 2. The data indicate that the frequency and intensity of tropical cyclones (TCs) have gradually increased over the BoB in the North Indian Ocean (NIO) over the past four decades [74]. Genesis and landfall occurrences of TCs were estimated using the India Meteorological Department (IMD) best-track data, showing that 109 TCs made landfall over the

BoB from 1982 to 2020 (Figure 2a,b). Observations indicate that twenty-four extremely severe cyclonic storms and four super cyclonic storms were formed over the BoB (Figure 2a). TCs, formed over the BoB, had the highest landfall rates along the coasts of Odisha and West Bengal in the northwest BoB, followed by Andhra Pradesh along the west-central BoB. Hotspot analysis identifies statistically significant areas of TC genesis. This analysis aggregates points of TC occurrence into polygons or clusters of points in close proximity based on calculated distances. The southeast BoB has been identified as a potential hotspot for TC genesis in the past 40 years. Specifically, for extremely severe cyclonic storms, the southeast BoB has been identified as a potential genesis region (Figure 2c). The tracks of ESCSs are displayed in Figure 2d, showing the transformation from very severe cyclonic storms into ESCSs near coastal areas, which significantly affected coastal communities in terms of property damage and loss of life. Rapid intensification (RI), defined as an increase in surface wind speed of 30 knots (15.4 m/s) or more within 24 h, was assessed for TCs using IMD best-track data. Findings show that 99% of ESCSs are rapidly intensifying cyclones. ESCSs that experienced RI from 1990 to 2021 are shown in Figure 2e. They reported trends in global tropical cyclone activity from 1990 to 2021 and highlighted the increasing trend of hurricane activity [80]. However, their study did not present linear trends of intense cyclones over the North Indian Ocean due to a lack of significant datasets. The present study highlights that the increasing number of intense tropical cyclones and the rising RI trend (1 per decade) of ESCSs over the North Indian Ocean are well correlated with them [80]. The ESCSs that have rapidly intensified in the recent decade are highlighted with red circles. These were analyzed in this study using the mesoscale WRF model and the IMDAA dataset for performance evaluation. According to [5,22], the duration and intensity of ESCSs over the BoB have shown an increasing trend over the past three decades (Figure 2f). This climatological analysis of ESCSs over the BoB highlights the need for a comprehensive study of these storms to enhance and customize the WRF model system at a mesoscale.

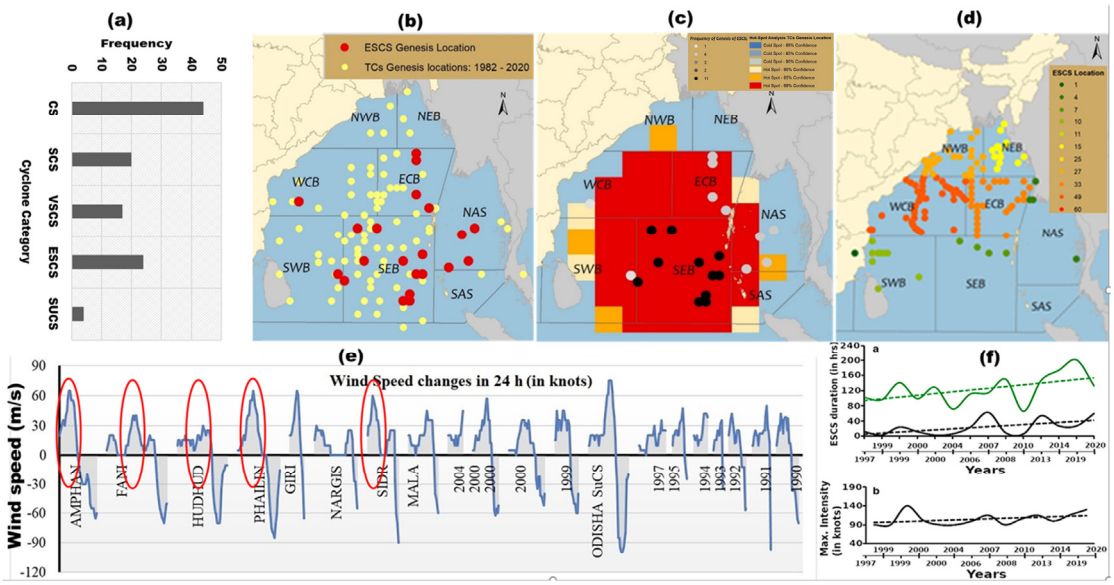

Figure 2. Climatological analysis of tropical cyclones over the Bay of Bengal (BoB) during 1982–2020, representing: (**a**) different categories of TCs and their frequency (CS: cyclonic storm, SCS: severe cyclonic storm, VSCS: very severe cyclonic storm, ESCS: extremely severe cyclonic storm, SUCS: super cyclonic storm), (**b**) genesis locations of ESCSs (Marked in Red), (**c**) hotspots of TCs genesis locations, (**d**) tracks of ESCSs, (**e**) rapid intensification of ESCSs (red ovals—Amphan, 18 May 2020 at 00UTC; Fani, 30 April 2019 at 03UTC; Hudhud, 11 October 2014 at 06UTC; Phailin, 10 October 2013 at 06UTC; Sidr, 13 November 2007 at 00UTC), and (**f**) trend analysis of ESCS duration and intensity (Source: [5,22]).

3.2. Key Synoptic Features During the Life Cycle of Tropical Storms

We have analyzed key synoptic features, such as atmospheric and large-scale flows in terms of geopotential height (m), relative humidity (%), and wind vectors at 850 hPa from ERA5 data at 00 UTC, during the life cycle of five ESCSs over the North Indian Ocean (Figure 3). In the case of Cyclone Amphan, the low-pressure trough gradually increases from the pre-cyclonic stage to the intensification stage, as indicated by the closed geopotential contours. This signifies the development of a well-defined core structure of the cyclone. High relative humidity (>80%) is observed from the formation stage to the intensification stage. The strong wind flows are observed from the south and southwest to the northeast, transporting moist air to fuel the storm's convection (Figure 3(a1–a5)). For Cyclone Fani, a strong low-pressure trough is observed during the intensification stage, along with the dynamic variations in the radius of the cyclonic eye. Strong winds flow from the southwest, carrying significant moisture to sustain the convection process. A well-defined circulation is also observed on the right side of the cyclone's center (Figure 3(b1–b5)). In the cases of Cyclones Hudhud and Phailin, the low-pressure systems originate near the Andaman Islands and gradually move toward the east coast of India. This movement is accompanied by increased relative humidity near the storm centers and strong circulation flows from the southeast. Additionally, a high-pressure system located northeast of the storms influences their movement toward the east coast of India, dynamically altering the radius of the cyclonic eyes (Figure 3(c1–c5,d1–d5)). Similarly, for Cyclone Sidr, the low-pressure system moves from the southeast to the northeast, as indicated by the concentric closed contours of geopotential height, with relative humidity of 90%. Strong, large-scale flows, represented by wind vectors, are observed northeast of the storm area (Figure 3(e1–e5)). The synoptic features clearly showed the progression of the storms from the depression stage to the landfall stage, characterized by strong circulation features, high relative humidity, and dynamic variations in the storm eyes. This analysis highlights the critical role of large-scale forcing in predicting cyclonic tracks and shows how high relative humidity at lower levels facilitates the intensification of storms by deep moisture transport.

3.3. The Performance of Model Forecast

Figure 4 displays the initial low-pressure vortex of five ESCSs: Amphan, Fani, Hudhud, Phailin, and Sidr. This was derived from the IMDAA dataset and compared with the IMD best-fit track data, with the location indicated by a weather symbol. Additionally, initial positional errors were calculated and are represented in the bar graph (Figure 2). This study revealed minor errors concerning IMD data in predicting the low-pressure vortex locations of storms, Amphan, Fani, and Hudhud (86.6 km, 35 km, and 47 km, respectively). But, the errors for Phailin (120 km) and Sidr (127 km) were major ones. Several reasons could account for these large errors, as listed below:

- IMDAA data have a limitation in capturing fine-scale features, such as the location and structure of the low-pressure vortex, due to its horizontal resolution of 12 km at the initial stage.
- IMDAA data are prepared using 4D-Var data assimilation, and its initial conditions depend on the availability, density, and quality of observational data over the TC genesis locations. These large errors may be caused by a lack of observational data over the genesis locations in the Bay of Bengal.
- The temporal resolution of the IMDAA data is available at 6 h intervals, which might result in the loss of rapid changes in the cyclone's position and structural features.

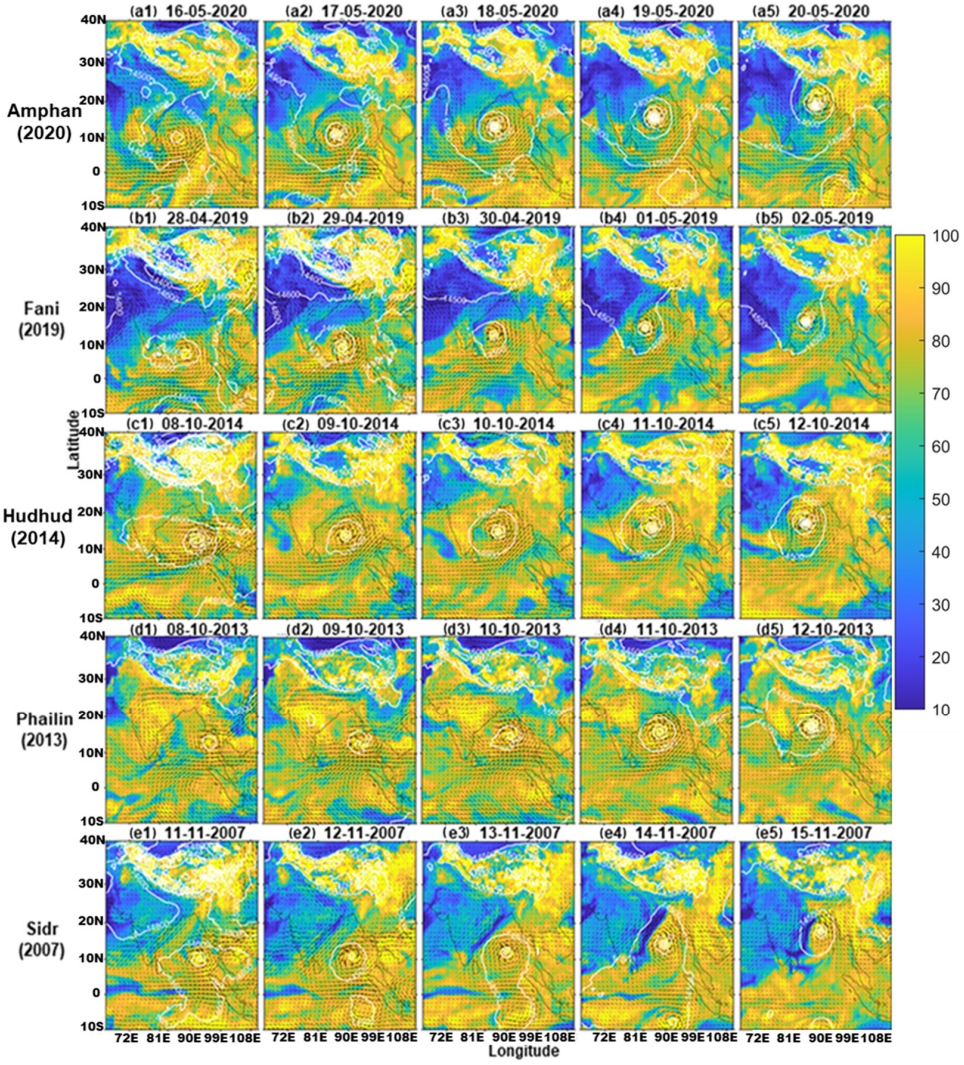

Figure 3. Synoptic features in terms of atmospheric conditions and large-scale flows, including geopotential height (in contours), relative humidity (shaded), and wind vectors at 850 hPa from ERA5 analysis at 00 UTC during the life cycle of cyclonic storms: (**a1**–**a5**) Amphan; (**b1**–**b5**) Fani; (**c1**–**c5**) Hudhud; (**d1**–**d5**) Phailin; (**e1**–**e5**) Sidr.

Figure 5 presents the model's simulated tracks of the five ESCSs using the IMDAA dataset compared with the IMD best-fit track. The results showed that the simulated tracks of Hudhud, Phailin, and Fani, using the IMDAA dataset, were well captured and comparable to the IMD best-track data throughout the simulation period. In contrast, the simulated track of Amphan with the IMDAA dataset deviated to the right of the IMD track as it moved toward the northeast. Similarly, in the case of Cyclone Sidr, the model's simulated track for 96 h deviated more than other cyclones' tracks compared to the observational data. This deviation may be due to an initial positional error of the low-pressure vortex. Overall, results regarding tracks of five ESCSs suggest that the model performance has a good agreement with IMD best-track data with the least error in all cases. This good agreement is attributed to the better initial conditions in terms of the initial low-pressure vortex positional errors of approximately 47 km, 120 km, and 35 km for Hudhud, Phailin, and Fani cyclones, respectively. Though Cyclone Phailin had a high initial position error of low-pressure vortex, model simulated the better track compared to IMD best-track due to a minimal difference of 3 m/s wind speed between IMDAA data and the observational data at the model's initial state, lower values of vertical wind shear which triggers the initiation of a cyclonic storm in later stages, and high values

of relative humidity of approximately 90% in the mid-tropospheric level. In addition, the synoptic features showed a better representation of the cyclone's eye, formation of low-pressure system, structure and large-scale flows at the initial state. In contrast, other cyclones, such as Amphan and Sidr showed higher track simulation errors. The WRF model's failure to simulate the tracks of Amphan and Sidr was due to maximum positional errors of IMDAA data at initial time of model simulations. The maximum surface wind speeds (MSW, in m/s) of Amphan and Sidar cyclones at the model's initial state were approximately 16 m/s and 20 m/s from the IMDAA dataset, whereas the MSWs of the IMD data were approximately 26 m/s and 15 m/s, respectively. This clearly indicates the underestimation and overestimation of MSW for both cyclones compared to the IMD best-fit track data. It was also observed that the vertical profile of horizontal wind speed showed major differences between the lower and upper atmosphere. Additionally, the vertical profile of relative humidity variations at 600 hPa was inconsistent at the initial state of both cyclones. Furthermore, limitations in the physical parameterization schemes, including the optimization of schemes better suited for simulations of TCs over the Bay of Bengal and the configuration of domain size, may have restricted upper-atmosphere circulations. The significant variations in the atmospheric parameters at the initial state contributed to the failure in simulating the tracks of the Amphan and Sidr cyclones.

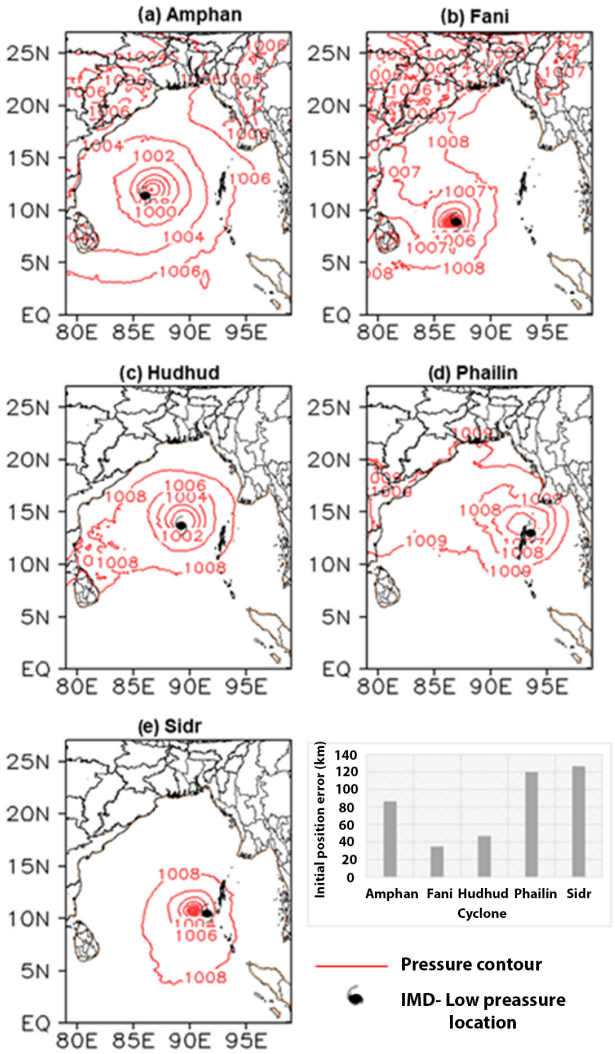

Figure 4. Initial low-pressure vortices of five ESCSs: (**a**) Amphan, (**b**) Fani, (**c**) Hudhud, (**d**) Phailin, and (**e**) Sidr—derived from the IMDAA dataset were compared with the IMD best-fit track data, indicating the location in the terms of the weather symbol.

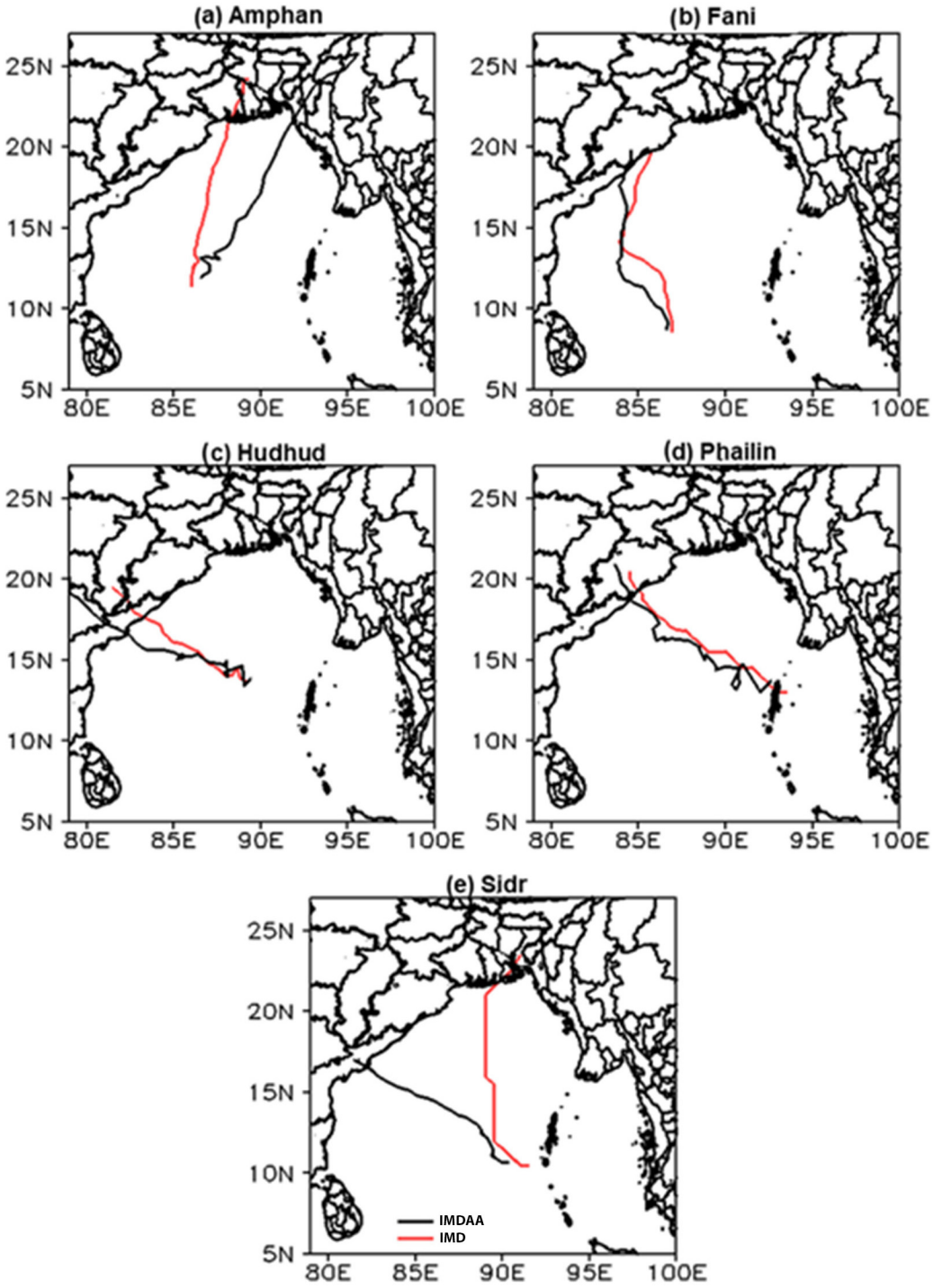

Figure 5. Model-simulated tracks of five ESCSs: (**a**) Amphan, (**b**) Fani, (**c**) Hudhud, (**d**) Phailin, and (**e**) Sidr along with IMD best-fit tracks.

Model simulations were conducted for a forecast period of 96 h. Along-track and across-track errors were calculated as the longitudinal and lateral distances, respectively, between the predicted track and the IMD best-track. These forecasted errors were then compared with the IMD best-track, representing the model's real-time forecast accuracy within this region. Figure 6 displays the model-predicted along- and across-track errors for five ESCSs, highlighting that the along-track error is consistently higher than the across-track error for all cyclones. Along-track errors for Fani, Hudhud, and Phailin varied between 50 and 300 km. But Amphan and Sidr along-track error varied between 50 and 1100 km. Across-track errors varied between 30 and 150 km for Fani, Hudhud, and Phailin

and between 50 to 700 km for Amphan and Sidr. Along- and across-track errors are more in the day 4 forecast of Amphan and Sidr. The model predictions indicated that across-track errors of all storms are lower compared to along-track errors. This can be attributed to synoptic features of atmospheric flow patterns and the nature of steering currents.

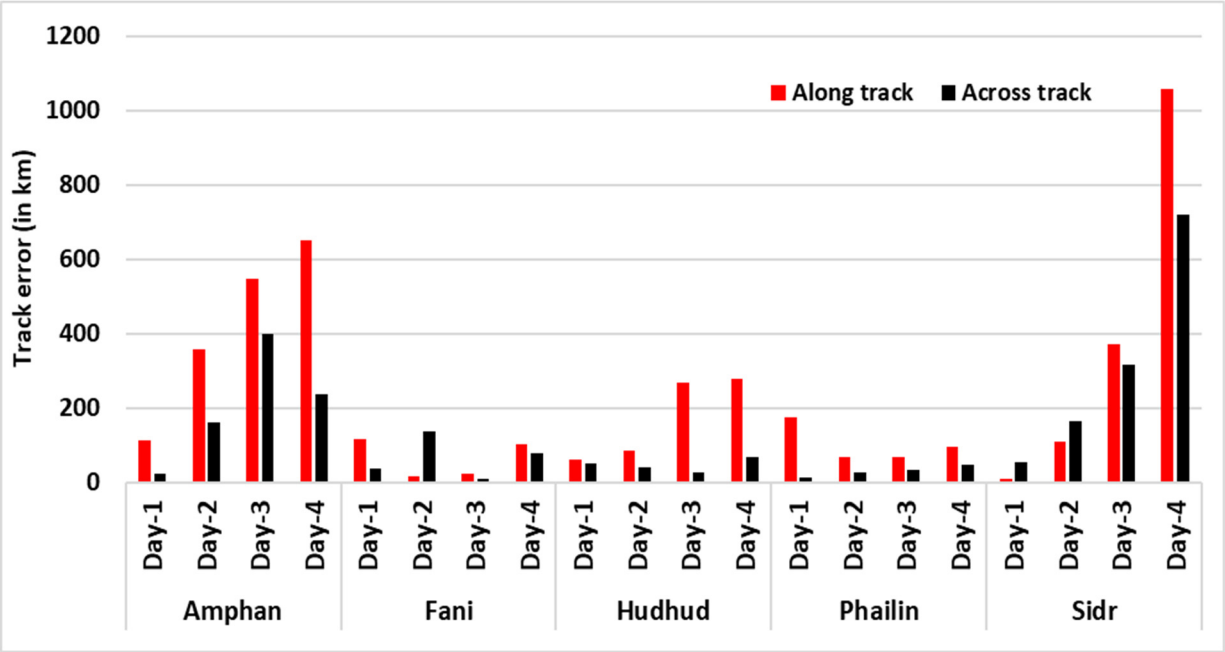

Figure 6. Temporal evaluation of along- and across-track errors for five ESCSs over the Bay of Bengal.

Figure 7 shows the temporal evolution of the model-simulated maximum sustained surface wind speed (MSW) using the IMDAA dataset for the five ESCSs and their comparison with the IMD best-fit track dataset. In the case of Cyclone Amphan, predicted MSW showed an underestimation of Cyclone Amphan intensity for periods between 0–48 h and 72–96 h. This also overestimated the storm's peak intensity during the 48–72 h forecast period. Similarly, in the Fani storm, simulated MSW initially over-predicted the intensity for the first 72 h and subsequently under-predicted it until its dissipation. For Cyclone Hudhud, the forecasted MSW followed a similar pattern to the IMD up to 72 h. In the case of Cyclone Phailin, the predicted intensity well followed the IMD track data for the first 24 h. After that, the cyclone intensity was under-predicted. Finally, during Cyclone Sidr, the model-simulated MSW is well matched with the IMD throughout its forecast period compared to the other cyclones. It was concluded that there is good agreement between model predictions in intensity forecasts and IMD best-track data in most cases.

Figure 8 displays the simulated wind fields during the intensification of five ESCSs, highlighting an apparent variation in wind speed around the eye of the cyclones ranging from 35 m/s to 70 m/s for all cyclones, except for the Sidr cyclone. The model-simulated wind fields during intensification were compared to the IMD best-track data. They were evaluated statistically using absolute bias, which varied from 3 to 11 m/s (Table 4). The statistical analysis revealed that the absolute bias is less than 10 m/s for all cyclones compared to the IMD dataset, indicating a good agreement between model predictions and the IMD dataset.

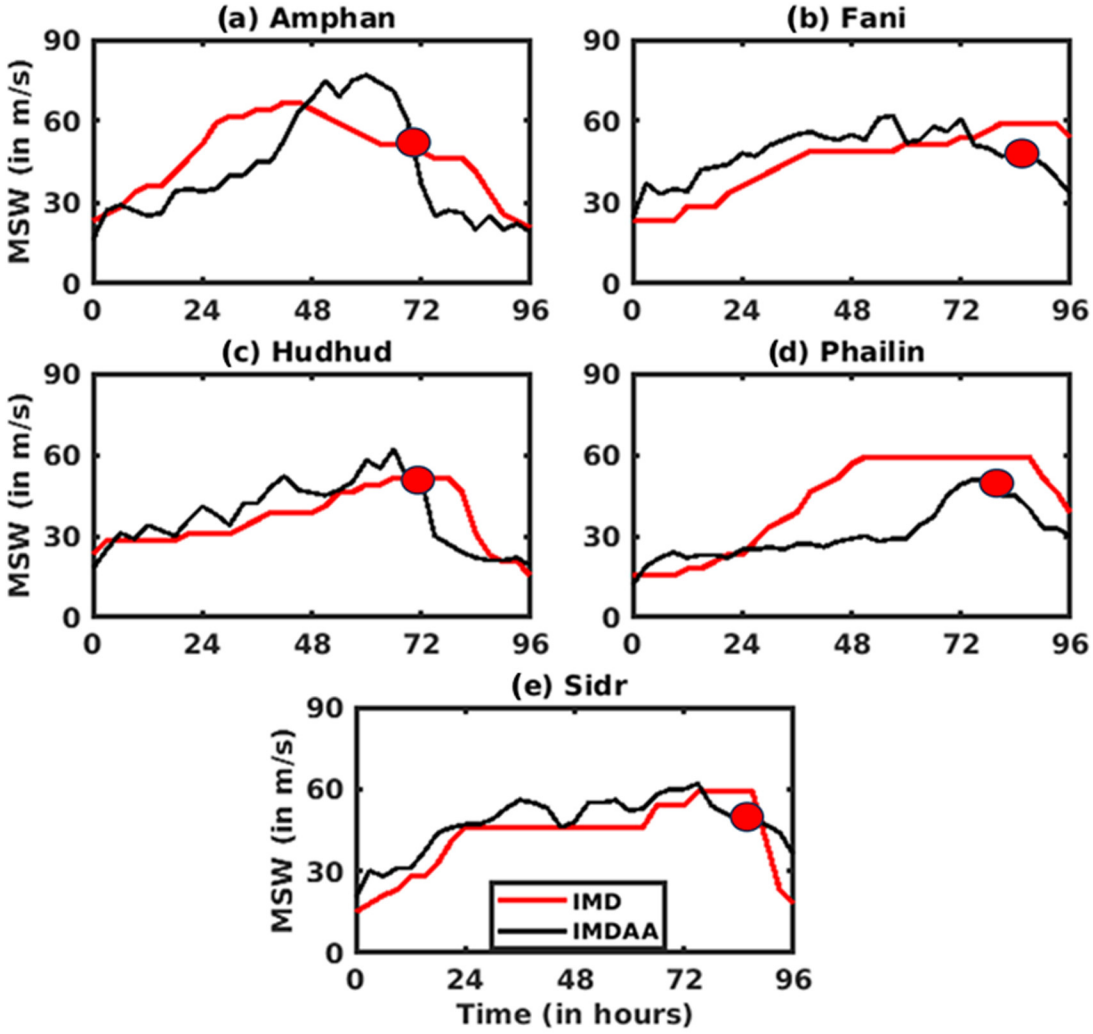

Figure 7. Temporal variation in model-simulated MSW (in m/s), (**a**) Amphan, (**b**) Fani, (**c**) Hudhud, (**d**) Phailin, and (**e**) Sidr along with the IMD best-fit track dataset.

Table 4. Model-simulated wind fields during the intensity stage and before the landfall stage and their absolute bias with the IMD dataset for five ESCSs over the BoB.

Cyclone	Wind Fields (m/s) During Intensity Stage			Wind Fields (m/s) Before Landfall		
	IMD	Model	Absolute Bias	IMD	Model	Absolute Bias
Amphan	66.87	77	10.13	45	70	25
Fani	59.15	62	2.85	57.5	48	9.5
Hudhud	51.4	62	10.6	50	55	5
Phailin	59.15	51	8.2	57.5	51	6.5
Sidr	59	62	3	57.5	49	8.5

Figure 9 displays the simulated wind fields before the landfall of five ESCSs, highlighting a clear variation in wind speed ranging from 25 m/s to 50 m/s for all cyclones, except for Cyclone Amphan. The model-simulated wind fields before landfall were then compared to the IMD best-track data and evaluated statistically using absolute bias, ranging from 5 to 25 m/s (Table 4). The statistical analysis revealed that the absolute bias is less than 10 m/s for most cyclones compared to the IMD dataset, indicating a good agreement. The discrepancy is that the updated lateral boundary data at 6 h intervals may not have adequately captured the evolving synoptic features of the atmosphere, leading to discrepancies in the

evaporation transport, radiative flux exchange, and overall intensity predictions. Further, there are limitations in the physical parameterization schemes, including the optimization of schemes better suited for simulations of TCs over the Bay of Bengal and the domain size configuration, which may have restricted upper-atmosphere circulations.

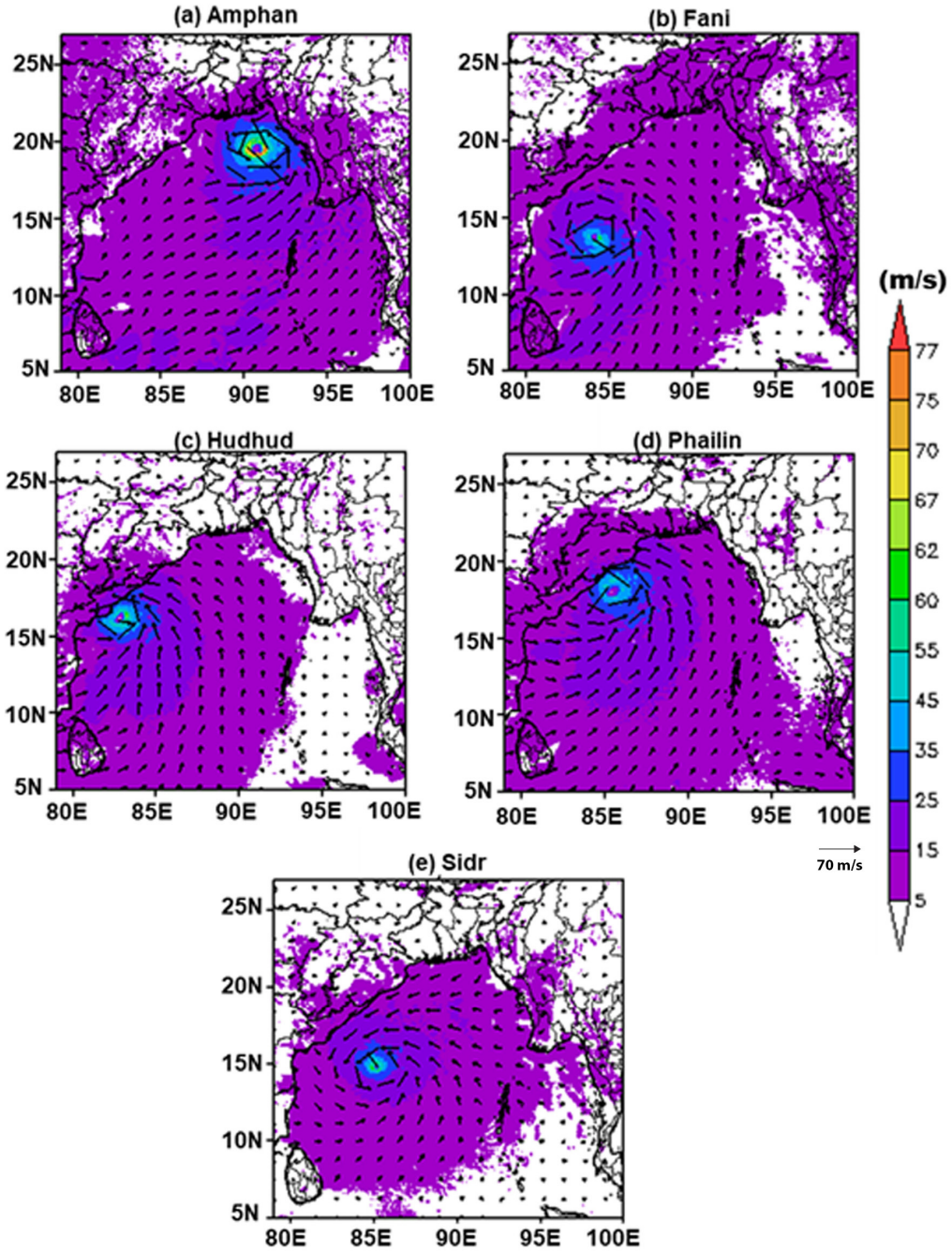

Figure 8. Simulated wind fields (m/s) during intensification of ESCSs: (**a**) Amphan; (**b**) Fani; (**c**) Hudhud; (**d**) Phailin; and (**e**) Sidr.

Table 5 details the comparison between the model-simulated Radius of Maximum Winds (RMW) and the IMD data. This illustrates that the RMW values were higher than those in the IMD dataset during day 1, gradually decreasing from day 1 to day 4. Notably, the RMW on day 3 is more comparable to the IMD dataset. It can be inferred that the prediction of RMW is generally comparable to the IMD. In the case of Cyclone Hudhud, the RMW difference exceeding 25% is attributed to the early intensification, formation of a small-sized eye, and occurrence of early landfall.

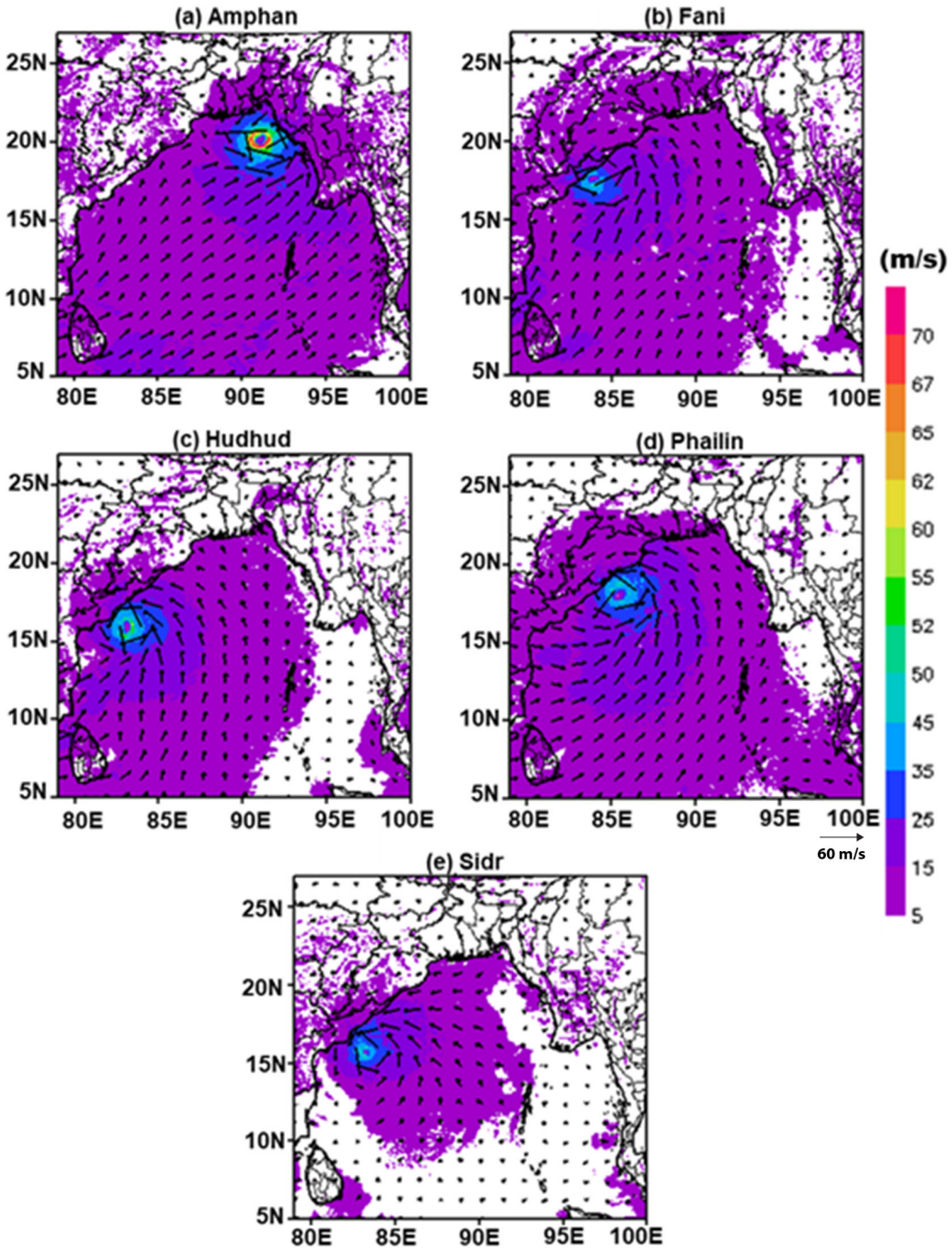

Figure 9. Simulated wind fields (m/s) before landfall of ESCSs: (**a**) Amphan; (**b**) Fani; (**c**) Hudhud; (**d**) Phailin; and (**e**) Sidr.

Table 5. Comparison between model-simulated RMW in km, and the IMD datasets for five ESCSs over the BoB.

Cyclone	RMW in km				Rmw Mean	IMD Mean
	Day 1	Day 2	Day 3	Day 4		
Amphan	36.6	20.7	42.3	LF*	33.2	32.9
Fani	25.1	22.7	22.3	44.0	28.5	30.5
Hudhud	31.7	28.9	27.1	LF*	29.2	37.4
Phailin	50.5	45.6	28.8	49.5	43.4	38.8
Sidr	25.7	26.1	22.0	37.8	27.9	35.6

LF*—landfall occurred.

The model simulated the rapid intensification (>15.4 m/s) and dissipation (−15.4 m/s) of the five cyclones in a 24 h period using IMDAA data (Figure 10). This was compared with IMD's estimated intensification from their best-fit track data. The model simulation for Cyclone Amphan overestimated the rapid intensification phase for 48 h and underestimated the rapid dissipation phase during 72–96 h. Similarly, in the case of Cyclones Fani, Hudhud, and Sidr, model simulations reasonably well captured the trend of rapid intensification and dissipation. Cyclone Phailin was under-predicted for the first 70 h, but thereafter, it was over-predicted rapid dissipation. One major reason why the model simulation fails to capture Phailin's rapid intensification is the lack of significant development in vertical wind shear between 850 and 200 hPa. This is attributed to the model's inability to resolve the storm's internal structure and the eye of the cyclone. This is also associated with the influence of diabatically driven circulations interacting with the trough–jet storm system. Overall, the results suggested that the model can capture the rapid intensification well with IMD in most of the cyclones.

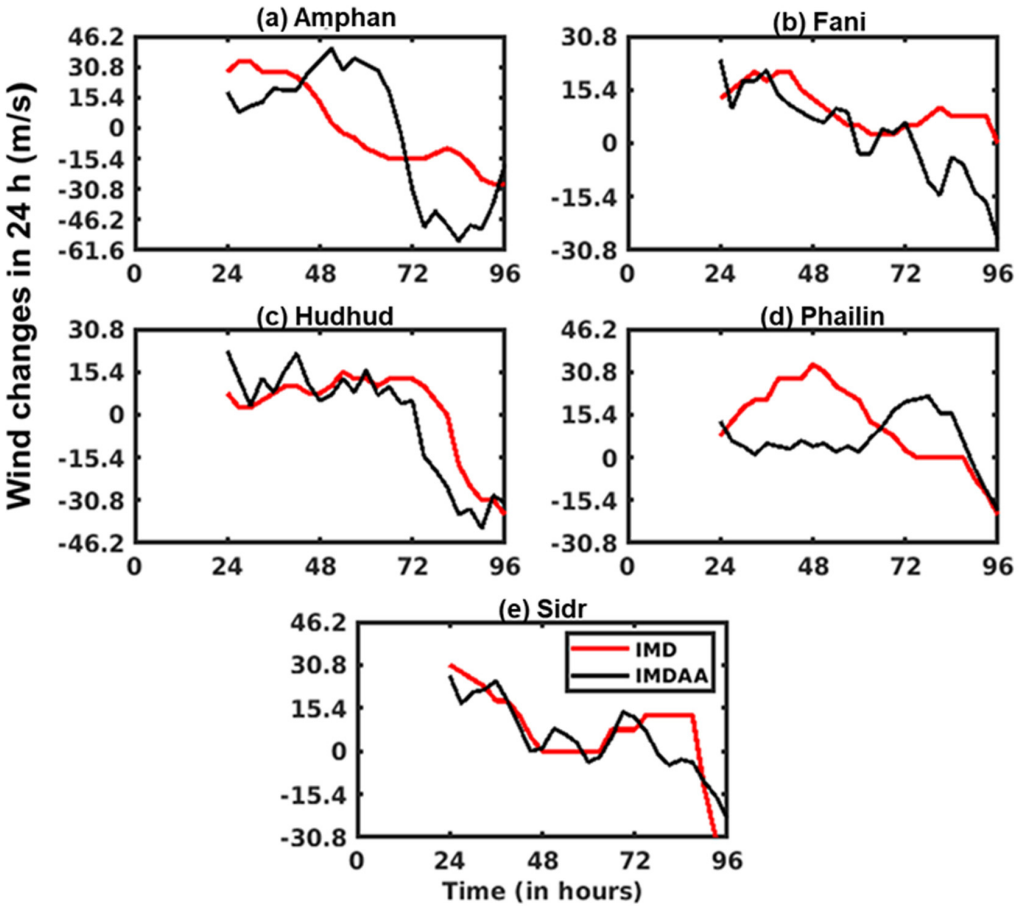

Figure 10. Wind speed changes in 24 h (in m/s) for five ESCSs from model simulations and the IMD best-fit track dataset: (**a**) Amphan, (**b**) Fani, (**c**) Hudhud, (**d**) Phailin, and (**e**) Sidr.

Figure 11 shows the temporal variation in model-simulated central sea level pressure (CSLP) using the IMDAA dataset for the five ESCSs and their comparison with IMD CSLP. It is observed that the model-predicted CSLP is well matched with IMD in Cyclones Fani, Hudhud, and Sidr. On the other hand, the model showed a trend of over-prediction and under-prediction in Cyclones Amphan and Phailin, respectively. Finally, it is concluded that the good agreement with the IMD best-track data in predicting CSLP for most cyclones was primarily due to the model's precise depiction of the initial low-pressure system's vortex, which minimized deviations from the actual storm evolution. The minimal distance

errors of low-pressure vortices may be attributed to improved prediction of pressure drop and reduced track errors.

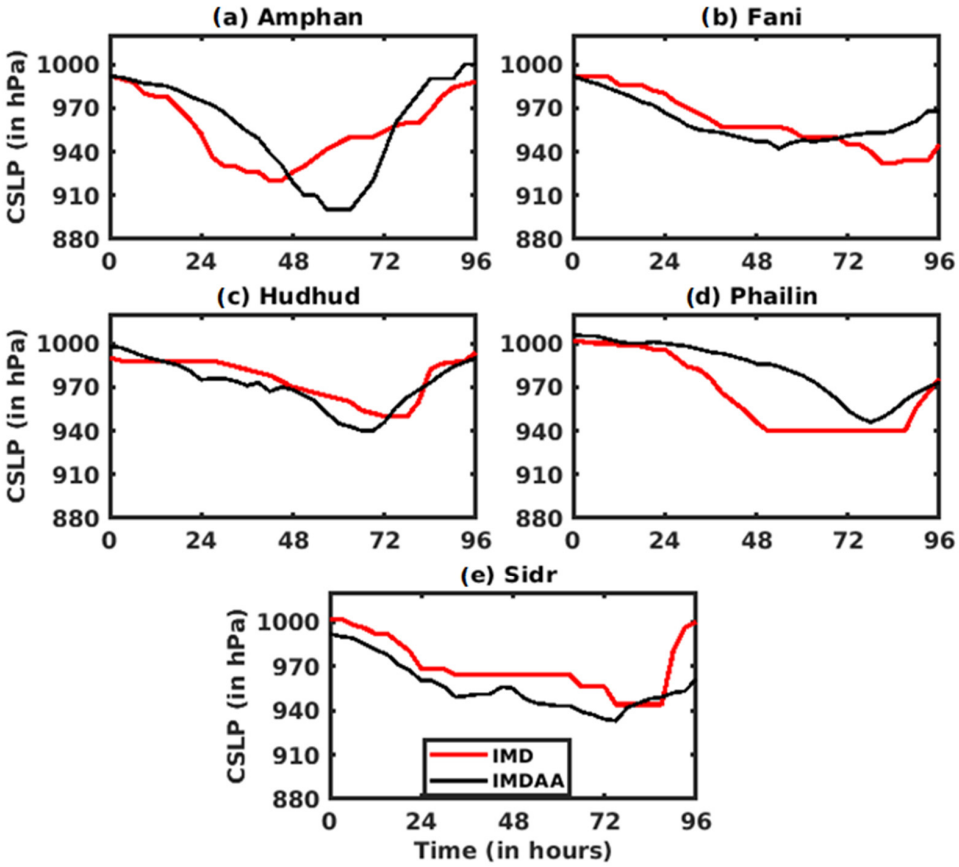

Figure 11. Temporal variation in model-simulated central sea level pressure (CSLP) for five ESCSs: (**a**) Amphan, (**b**) Fani, (**c**) Hudhud, (**d**) Phailin, and (**e**) Sidr, along with the IMD best-fit track dataset.

Model-simulated Convective Available Potential Energy (CAPE) is computed as the area-averaged value over a $4^\circ \times 4^\circ$ latitude–longitude box centered on the cyclone's position. Similarly, model-simulated vorticity is computed at the 850 hPa pressure level, averaged over the same $4^\circ \times 4^\circ$ latitude–longitude region around the cyclone center. Table 6 presents the model-simulated CAPE (J/kg), vorticity (s^{-1}), and a comparison with the IMDAA dataset. The percentage difference in CAPE between the model-simulated and IMDAA datasets distinctly reveals that Sidr and Hudhud exhibited higher values (112% and 62%, respectively) compared to other storms. Similarly, when examining the vorticity (s^{-1}) for the Fani storm, the comparison between the model-simulated and IMDAA datasets revealed a notable percentage difference (30%) compared to other cyclonic storms. Overall, the comparison of CAPE and vorticity parameters between the model-simulated and IMDAA datasets showed a close match with most cyclonic storms.

3.4. Evaluation of Model Predictions Using Statistical Methods

Table 7 presents the daily estimated errors in the model simulation for five cyclones using IMDAA data. This includes track errors (in km), the absolute error of maximum surface wind (MSW) (in m/s), and the absolute error of central sea level pressure (CSLP) (in hPa). On day 1, all cyclones showed minimal errors in track prediction, whereas high errors in MSW and CSLP were observed. Thereafter, MSW and CSLP showed minimal errors on day 2 and day 3 compared to day 1. Mainly, the track errors of Fani, Hudhud, and Phailin showed the least errors from day 1 to day 4 compared to Amphan and Sidr. However, errors consistently increased day by day in Amphan and Sidr, as presented in

Table 7. The mean track errors using 3 h data for five ESCSs were approximately 356 km, 132 km, 165 km, 101 km, and 392 km, respectively. It is concluded that Fani, Hudhud, and Phailin predicted with fewer errors due to minimal deviations in their initial low-pressure cyclonic vortex position from the IMD data.

Table 6. The comparison model-simulated CAPE (J/kg) and vorticity (s^{-1}) with IMDAA dataset for five ESCSs.

Cyclone	CAPE (J/kg)			Vorticity (10^{-5} s^{-1})		
	Model	IMDAA	Absolute Difference in %	Model	IMDAA	Absolute Difference in %
Amphan	2175.80	1785.50	21	4.68	4.24	10
Fani	1938.66	2347.80	17	3.59	2.75	30
Hudhud	1994.20	1229.47	62	4.09	3.99	2
Phailin	1548.25	1175.56	31	3.95	3.44	14
Sidr	1497.81	705.44	112	3.26	2.63	23

Table 7. Model-simulated track errors (in km), absolute MSW error (in m/s) and absolute CSLP errors (in hPa) for all five ESCSs.

	Day 1	Day 2	Day 3	Day 4	Mean Errors (Using 3 Hourly Data)
Track errors (in km)					
Sidr 2007	53	196	489	1282	356
Phailin 2013	175	72	74	105	132
Hudhud 2014	77	94	269	285	165
Fani 2019	150	138	25	129	101
Amphan 2020	114	393	677	677	392
Mean errors	114	179	307	496	229
MSW errors (in m/s)					
Sidr 2007	0.7	1.7	5.9	18.5	7
Phailin 2013	1.8	27.5	10.1	8.5	13.9
Hudhud 2014	10.1	7.4	0.4	3.5	6.7
Fani 2019	12	6.1	6.9	21	9.1
Amphan 2020	17.4	3.7	11.8	1.5	12.9
Mean Absolute Errors	8.4	9.3	7	10.6	9.9
CSLP errors (in hPa)					
Sidr 2007	8	9	22	39	14.6
Phailin 2013	4	40	14	3	17
Hudhud 2014	13	2	4	4	7.7
Fani 2019	13	10	6	23	10.6
Amphan 2020	23	7	14	12	19.1
Mean Absolute Errors	12.2	13.6	12	16.2	13.8

The absolute error of MSW (in m/s) calculated daily is presented in Table 7. The results show that in most cyclones, absolute wind errors were decreasing from day 1 to day 3 compared with the mean error of MSW for most of the cyclones. However, on day 2, Phailin was predicted with a higher error value (27.5 m/s). The mean absolute wind speed errors from day 1 to day 4 for five ESCSs were 8.4 m/s, 9.3 m/s, 7 m/s, and 10.6 m/s, respectively. It is seen that the model produced less error on day 3 compared to other

days, showing a better forecast in terms of intensity. It is concluded that the IMDAA data performed well regarding the MSW.

Table 7 also shows the absolute error of the CSLP (in hPa) every 24 h. It is seen that the simulated CSLP errors are decreasing compared to day 1 for most storms and are calculated as an average value over 24 h. This clearly indicates that CSLP errors decreased when the depression stage transformed into an intense storm. However, Phailin and Sidr produced higher error values on days 2 and 4. The mean absolute CSLP errors from day 1 to day 4 for five ESCSs were 12.2 hPa, 13.6 hPa, 12 hPa, and 16.2 hPa, respectively. It is observed that day 3 showed negligible error. In case of Phailin, the MSW and CSLP errors during Days 1–2 can be attributed to inaccuracies in the representation of the storm's structure on day 2, the low-pressure vortex position at initial state and minor difference of wind speed. Additionally, the updated lateral boundary data at 6 h intervals may not have adequately captured the evolving synoptic features of the atmosphere, leading to discrepancies in the evaporation transport, radiative flux exchange, and overall intensity predictions. These factors possibly contributed to errors in MSW and CSLP estimates during the early forecast period. Overall, regarding the CSLP, the IMDAA data performed better and more accurately for most cyclones.

The model's performance was also evaluated from the outcome of the 4 km horizontal resolution of model simulations using a Taylor diagram, considering the Root Mean Square Error (RMSE), the Normalized Standard Deviation (NSD), and the Correlation Coefficient (CC). This evaluation was conducted for parameters such as MSW and CSLP of five ESCSs by comparing the model forecasts with IMD best-track data. The Taylor diagrams (Figure 12a–e) depict the relative skill of the model's forecasted MSW for the 5 ESCSs compared to IMD best-track data. The CC of MSW predicted by model simulations ranged between 0.9 and 0.7 for all the cyclones, except Cyclone Fani, where the CC of MSW prediction differed. The NSD of simulated MSW (below 1.0 m/s) is approximately equal to the observed NSD (around 1 m/s) for cyclones Fani, Hudhud, Phailin, and Sidr, except Amphan (1.5 m/s). Simulated MSW exhibited a high correlation with IMD data and a low RMSE for most cyclones. Similarly, the Taylor diagrams (Figure 12f–j) for the simulated CSLP using the IMDAA dataset showed high correlation values between 0.7 and 0.9 in all cases. The NSD of simulated CSLP (between 0.6 hPa and 1.5 hPa) with the IMDAA dataset was highly significant in comparison to the observed NSD for cyclones Hudhud and Sidr. At the same time, the observed NSD was lower for other cyclones, Amphan, Fani, and Phailin. Simulated cyclones exhibited low RMSE values (between 0.4 and 0.6 hPa) for most cyclones. The analysis of the Taylor diagram clearly showed the model's performance through the evaluation of the RMSE, CC, and NSD for the parameters of MSW and CSLP for five ESCSs over the Bay of Bengal. The CC values for MSW and CSLP varied from 0.7 to 0.9, indicating that the model predictions are in good agreement with the IMD best-track data. Similarly, the Normalized Standard Deviation (NSD) of MSW and CSLP parameters was below 1 for most storms, whereas higher values (approximately 1.5) were observed for a few storms, such as Cyclones Amphan and Sidr. This highlights the variability in the model's ability to capture the wind and pressure fields for different cyclones. The RMSE values in the Taylor diagram ranged between 0.4 and 0.7, indicating that the model captures cyclone intensity with minimal deviation from observed data. The Taylor diagram, along with the analysis of time-series tracks, maximum sustained wind speed, and central sea level pressure, demonstrated high model reliability. This also identified areas for further refinement to enhance accuracy, as evidenced by the high correlation, low RMSE, and minor deviations in NSD for specific cyclones.

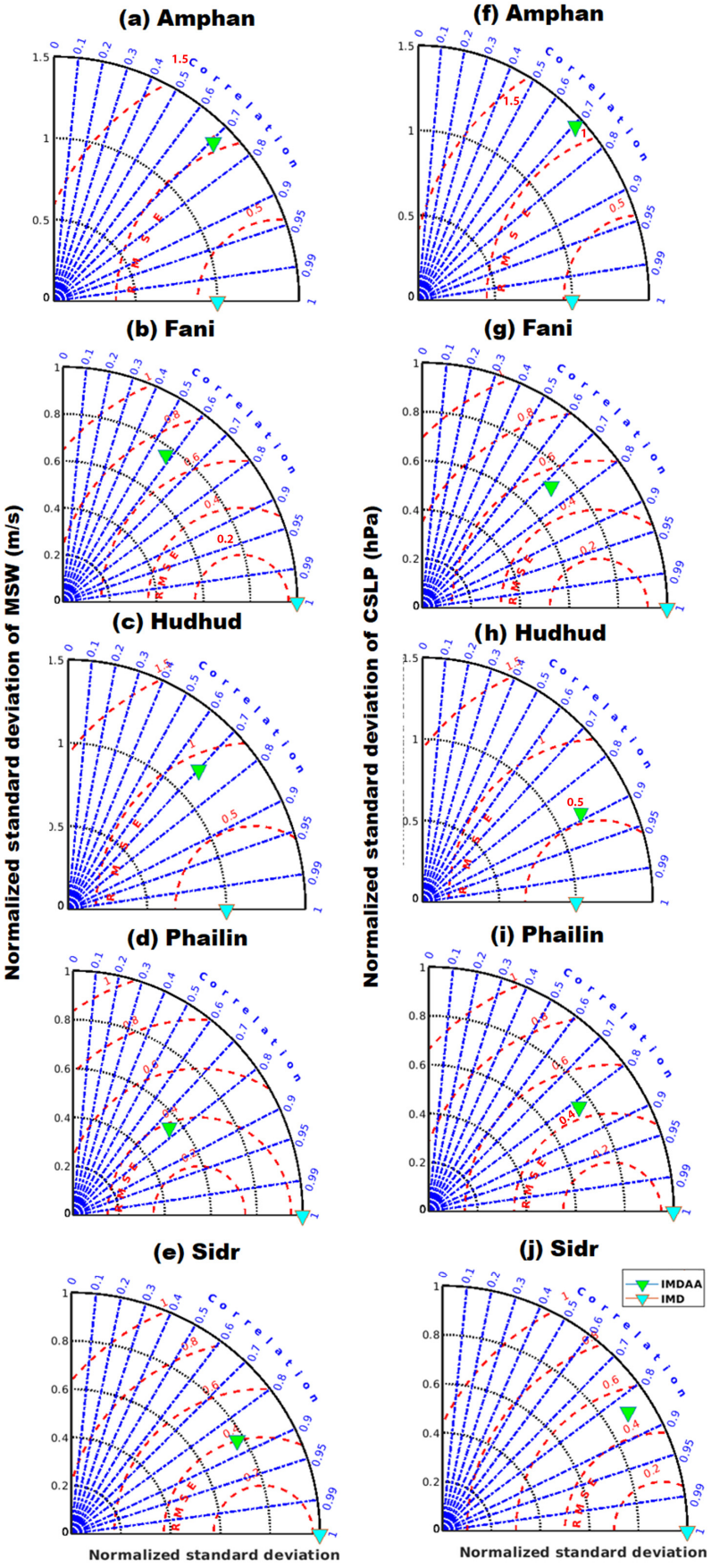

Figure 12. Taylor diagrams of MSW (**a**–**e**) and CSLP (**f**–**j**) for five ESCSs [(**a**,**f**) Amphan, (**b**,**g**) Fani, (**c**,**h**) Hudhud, (**d**,**i**) Phailin and (**e**,**j**) Sidr].

The simulation skill was calculated for the intensity and landfall in terms of the Brier Score (BS) and the Critical Success Index (CSI). The results pointed out that the BS was approximately 0.014 (BS = 0 is good indicator) and indicated a very good performance, while the simulated CSI score is approximately 0.67 (CSI = 1 is a good indicator), indicating a moderate prediction of landfall.

3.5. Evaluation of the Rainfall and Structure of Storm Forecasts

Model simulations were performed to forecast the 24 h accumulated rainfall for five ESCSs and were compared with the 24 h accumulated rainfall of TRMM data (Figure 13). The model predicted that the 24 h accumulated rainfall varies between 100 and 650 mm/day, and the spatial distribution is well matched with the TRRM data at the particular period of the individual storms.

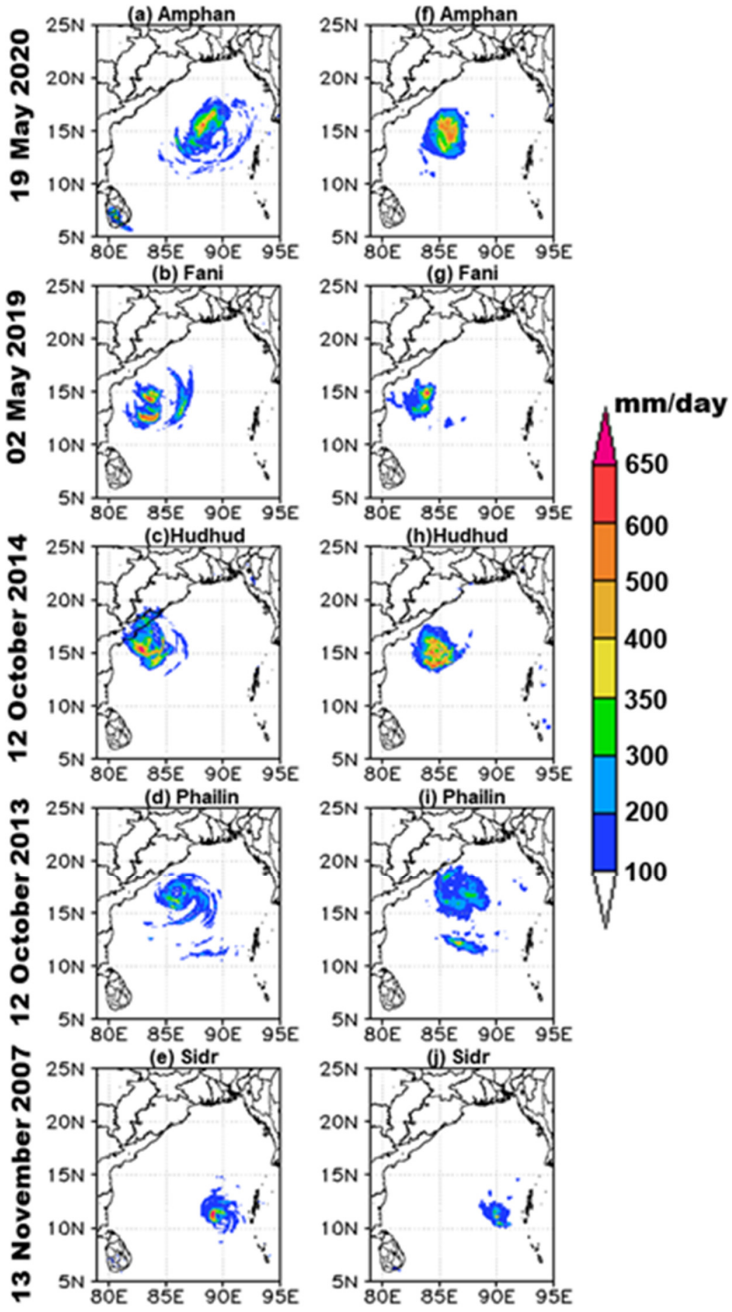

Figure 13. Accumulated rainfall (in mm/day) over 24 h for the five ESCSs presented as (**a**–**e**, **left** panel) model-simulated, and (**f**–**j**, **right** panel) TRMM rainfall data.

The 24 h accumulated rainfall (in mm/day) from Day 1 to Day 4 for all ESCSs is described in Supplementary Figures S1–S5. The accumulated rainfall results were compared with the high-resolution (11 km) TRMM datasets (https://giovanni.gsfc.nasa.gov/giovanni/ accessed on 14 January 2023). In the case of Super Cyclone Amphan (Supplementary Figure S1), the WRF model resolved well the magnitude of maximum rainfall. Still, the spatial distribution differed from Day 1 onwards due to the cyclone's movement. After Day 1, the simulated track deviated to the right of the observed track, causing the spatial distribution of daily rainfall to veer towards the side of the TRMM accumulated rainfall. The simulated accumulated rainfall is also slightly higher than the TRMM values. On Day 2 and Day 3 (19 May and 20 May 2020), the observed maximum rainfall was approximately 600 mm, resolving well in the WRF model and presenting more than 600 mm of rainfall with a broader spatial coverage and higher magnitude.

For Cyclone Fani (Supplementary Figure S2), the model captured well the magnitude and spatial distribution of maximum rainfall from day 1 to day 3. However, on day 4, the simulated track deviated to the left of the observed track, resulting in the spatial distribution of daily rainfall deviating to the left of the TRMM accumulated rainfall. The simulated accumulated rainfall was slightly higher than the TRMM values on day 2. On day 2 (1 May 2019). The observed maximum rainfall was approximately 800 mm, which is well resolved in the WRF model, showing slightly more than 800 mm of rainfall. On day 3 (2 May 2019), two peaks of maximum rainfall observed in TRMM data are well matched in the model simulation.

For Cyclone Hudhud (Supplementary Figure S3), the spatial distribution of maximum rainfall is well captured in the model from day 1 to day 4, mainly due to a better track forecast. However, from day 1 to day 4, the magnitude of simulated accumulated rainfall was slightly higher compared to TRMM. On day 4, the simulated accumulated rainfall was observed over Andhra Pradesh and adjoining areas of Odisha and Chhattisgarh. In contrast, rain was observed over the coastal region of Andhra Pradesh and adjoining areas of Odisha. Day 3 (12 October 2014) results showed that TRMM accumulated rainfall was at a maximum, approximately 650 mm, well resolved in the WRF model. On day 1 and day 2 (10 and 11 October 2014), the simulated rainfall was higher compared to TRMM, but on day 3 and day 4, the model provided a better simulation in terms of space and magnitude.

Similarly, Supplementary Figures S4 and S5 show the accumulated rainfall for Cyclones Phailin and Sidr, respectively. In the case of Cyclone Phailin, the simulated results provided a better forecast on each day except the day 2. The observed maximum accumulated rainfall was approximately 550 mm on day 4 (13 October 2013), well resolved in the WRF model, but showed heavier rainfall over the state of Odisha compared to TRMM. The rainfall pattern, spatial coverage, and magnitude were well resolved on day 3 (12 October 2013) in both model and observations. However, for Sidr, model-simulated rainfall in terms of spatial distribution was good on day 1 and day 2 (13 and 14 November 2007) and had a higher magnitude compared to TRMM. On day 3 and day 4, the model failed to capture the spatial rainfall due to higher track error. Overall, the model simulation of the accumulated rainfall of Cyclone Hudhud matched with the TRMM observational data for most of the days, compared to the other cyclones.

A statistical evaluation was performed between the model-predicted precipitation and the TRMM dataset for five ESCSs during the 96 h forecast (Table 8). The model-predicted precipitation for Cyclones Amphan, Fani, Hudhud, and Phailin was 60% above the TRMM datasets. In contrast, the Sidr cyclone showed less than 50% agreement due to the deviation of the track. This indicated that the model predictions showed good agreement compared to the TRMM datasets.

Table 8. Statistical evaluation of the model predicted precipitation with the TRMM dataset for five ESCSs over the BoB for a forecast period of 96 h.

Cyclone	Precipitation in mm for the Forecast Period of 96 h		RMSE	SD	Correlation
	Model	TRMM			
Amphan	562.50	425.00	152.06	184.84	0.97
Fani	700.00	637.50	114.56	125.00	0.67
Hudhud	687.50	487.50	220.45	143.61	0.66
Phailin	470.00	437.50	105.94	75.00	0.82
Sidr	712.50	500.00	438.03	204.12	0.23

The statistical metric, the Probability of Detection (POD), is calculated to evaluate the performance of the model's simulated rainfall. For the Phailin cyclone, POD was calculated for the rainfall parameter by comparing forecasted rainfall with AWS observations across 174 locations. The POD value was 96% for moderate rainfall (defined as 35.6–64.4 mm/day) and 80% for heavy rainfall (defined as 64.5–124.4 mm/day). A similar analysis was performed for other storms, comparing model forecast rainfall with the TRMM dataset, and similar results were obtained. This metric indicates that the model outperforms predicting rainfall using the IMDAA dataset.

Figure 14 shows the temperature anomaly obtained from model simulation and satellite observations for all ESCSs. Amphan was considered at 00 UTC on 19 May 2020, Fani at 03 UTC on 2 May 2019, Hudhud at 12 UTC on 11 October 2014, Phailin at 12 UTC on 11 October 2013, and Sidr at 03 UTC on 15 November 2007. The positive (negative) anomaly indicates the temperature is warmer (cooler) than the normal temperature. For the model, it is calculated as the temperature at a given time minus the average temperature during the entire simulation period [58].

From satellite observation, it is noticed that in most cyclone cases, the maximum warm core height varies from 9 km to 15 km. In model simulation, this phenomenon is observed at height between 4 km and 14 km. In the Amphan case, the maximum temperature anomaly was approximately 7 °C at approximately 12 km height, but in the model simulation, the anomaly was approximately 9 °C at approximately 10 km height. For Fani 2019, this value in observation was approximately 6 °C, but in the model simulation, the maximum temperature anomaly was approximately 8 °C. Similarly, this pattern in Hudhud-2019, Phailin 2013, and Sidr 2007 was noticed, with approximately 5 °C, 4 °C, and 4 °C in the observations and approximately 4 °C, 4 °C, and 10 °C in the model simulations, respectively. Results also highlighted that the model-simulated anomaly is stronger than observation. Overall, results suggest that the model's warm core structure was well resolved. However, the warm core structure was observed at a slightly lower level compared to the satellite observations.

Figure 15 depicts the model-simulated maximum reflectivity (in dBZ) for the Hudhud cyclone valid at 1500 UTC, 1800 UTC, and 2100 UTC on 11 October 2014. This was compared with DWR images obtained from the IMD Visakhapatnam DWR station. The forecasted intensity in terms of the MSW of Cyclone Hudhud showed a better prediction compared to the other ESCSs. Hence, the Hudhud case was selected to evaluate the performance of the model in simulating storm structure and size.

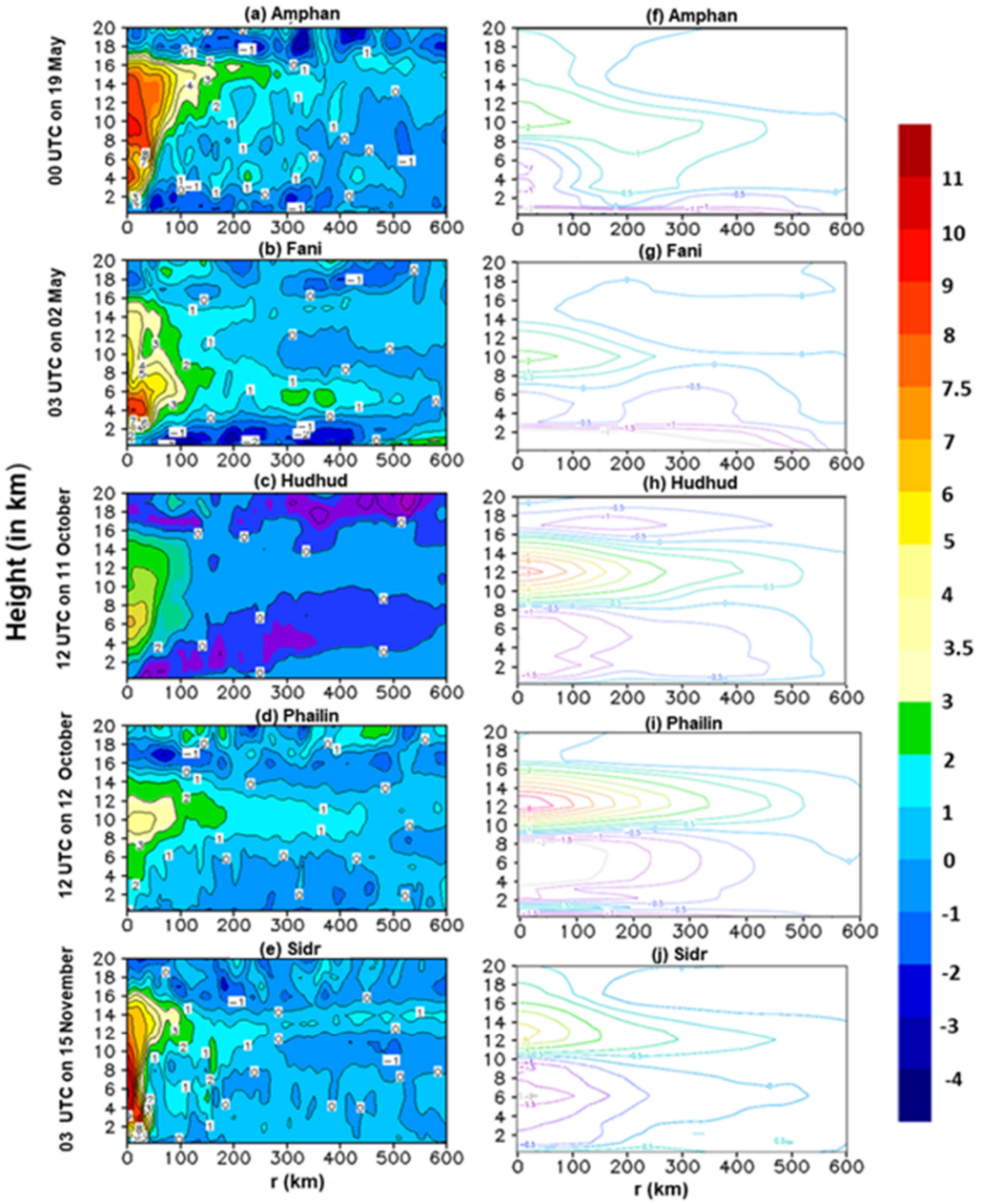

Figure 14. Temperature anomaly for five ESCSs, namely (**a**) Amphan at 00 UTC on 19 May 2020, (**b**) Fani at 03 UTC on 2 May 2019, (**c**) Hudhud at 12 UTC on 11 October 2014, (**d**) Phailin at 12 UTC on 11 October 2013, and (**e**) Sidr at 03 UTC on 15 November 2007 obtained from model-forecasted (**left** panel) and compared with satellite observations (**f–j**, **right** panel), respectively.

According to the report of the Regional Specialized Meteorological Centre (RSMC), it is suggested that at 1500 UTC, 1800 UTC, and 2100 UTC, the shape of the eye is closed. The size of the eye is approximately 38.1 km, 40.6 km, and 40.8 km, respectively, which approximately matches the model forecast with a slight deviation. The model simulations capture the eyewall cloud and spiral rain band well, as observed in DWR reflectivity images. Results from DWR images point out that the maximum convective bands in the wall cloud region were limited, starting from the west sector to the adjoining northwest sector around the center of the storm Hudhud during this period. It is also noted that the outer rain band is vital for rainfall activity along the region over the coastal region of Andhra Pradesh and the adjoining coastal region of Odisha. In the model simulation, the movement of the storm was slightly faster compared to the observed, and hence, the cloud band covers most of the coastal Andhra Pradesh and the adjoining coastal region of Odisha. In conclusion, the

model predictions demonstrate the storm's maximum reflectivity in terms of the size of the eye, eyewall, and rain bands, which are well resolved in the WRF model using the IMDAA reanalysis datasets.

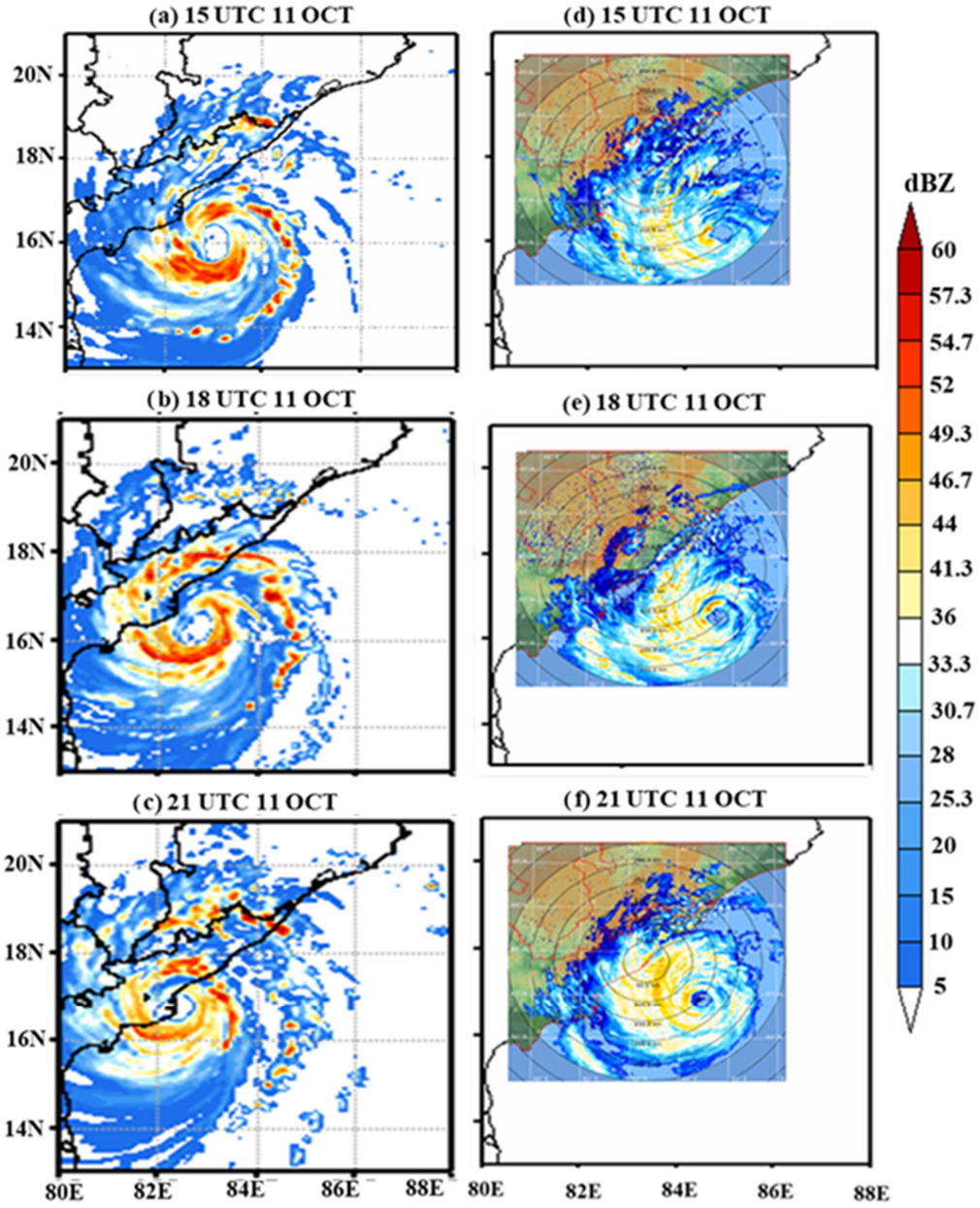

Figure 15. Simulated maximum reflectivity (in dBZ) for the Hudhud cyclone at (**a**) 1500 UTC, (**b**) 1800 UTC, and (**c**) 2100 UTC on 11 October 2014 (**a**–**c**) and are compared with the DWR images of Vishakhapatnam (**d**–**f**).

The climatological characteristics of tropical cyclones were analyzed in the present study, which highlighted the frequency of extremely severe cyclonic storms gradually increasing in recent decades. This trend is clearly supported by the observations of [74], who demonstrated the statistical significance of high-intensity storms by showing an increase in track length and residence time over the North Indian Ocean basin. They also highlighted a decreasing trend in the translational speed of high-intensity storms, estimated at approximately 2.5 km/h in recent decades. The performance of high-resolution (4 km) model simulations showed a better prediction of the track during the initial forecast days and improved intensity forecasting for most events. However, for a few events,

the track simulations were less accurate due to limitations in initial and lateral boundary conditions as well as the physical parameterization of the schemes [51,78]. Additionally, the tracking error of extremely severe cyclonic storms (ESCSs) gradually increased over the forecast period, which can be attributed to the inadequate representation of upper-air circulations and the updated lateral boundary conditions in the IMDAA data [81]. The IMDAA reanalysis data demonstrated good capability in capturing the mean, interannual, and intra seasonal variability of rainfall [71]. This is fairly reflected in the model-simulated precipitation, which correlates approximately 60% with TRMM rainfall data.

This study had a few limitations in predicting the operational parameters due to the deviations in the position of the low-pressure vortex and the initial intensity of the low-pressure system. Deviations in the initial position of the low-pressure vortex and biases in the storm's intensity may result in significant errors in forecasting ESCSs during the forecast period. Achieving accurate forecasts involves sensitizing the model configuration, particularly in terms of resolution, and providing accurate regional and global reanalysis datasets, as initial and lateral boundary conditions over the focused study region can improve storm simulations' accuracy and overall forecasting capabilities.

4. Summary and Conclusions

In this study, we conducted a climate analysis of tropical cyclones. We evaluated the performance of the mesoscale WRF modeling system using the IMDAA regional reanalysis dataset in predicting five extremely severe cyclonic storms (Sidr, Phailin, Hudhud, Fani, and Amphan) that developed over the Bay of Bengal during 2007–2020. A double-nested domain with a finer resolution of approximately 4 km in the WRF model was used for simulation, with a forecast period of 96 h. The simulated results are discussed using finer domains, validated with the IMD best-fit track datasets, TRMM daily accumulated precipitation, and satellite, AWS and Doppler weather radar observations. The outcomes of the present work are summarized as follows:

- Climatological analysis assessment showed that a total of 24 ESCSs formed over the BoB during the past three decades, and their trends in duration and intensity over the coastal regions are gradually increasing.
- This study revealed that the ESCSs' simulated tracks performed reasonably well for Fani 2019, Hudhud 2014, and Phailin 2013, but the model failed to capture the movement of the storms Amphan 2020 and Sidr 2007. This is due to the variations in dynamic and thermodynamic parameters such as the state of the initial low-pressure vortex, maximum sustained wind speed, vertical profiles of horizontal wind speed, and vertical profiles of relative humidity at the initial state of the storms. Furthermore, limitations in the adopted physical parameterization schemes for model simulations and domain size configuration may restrict upper-atmosphere circulations
- The mean track errors in the forecasted tracks of the five ESCSs from day 1 to day 4 using the IMDAA reanalysis datasets were approximately 114 km, 179 km, 307 km, and 496 km, respectively.
- The simulated MSW intensity of MSW was better for Fani 2019, Hudhud 2014, and Sidr 2007, with Mean Absolute Errors of approximately 9.1 m/s, 6.7 m/s, and 7 m/s, respectively.
- Mean Absolute Errors from day 1 to day 4 for MSW were 8.4 m/s, 9.3 m/s, 7 m/s, and 10.6 m/s, respectively, and were 12.2 hPa, 13.6 hPa, 12 hPa, 16.2 hPa, respectively, for CSLP with reference to the best-fit track data of IMD. The discrepancy might be in the updated lateral boundary data at 6 h intervals and inadequate capturing of the evolving synoptic features of the atmosphere, leading to differences in the evaporation transport, and radiative flux exchange.

- The simulated forecast of RI (wind speed changes approximately 15 m/s in 24 h) was better for Fani 2019, Hudhud 2014, and Sidr 2007. However, in the case of Phailin, the model was unable to capture RI due to the lack of significant development in vertical wind shear between 850 and 200 hPa and the evolution of the storm's internal structure and the eye of the cyclone. This is also associated with the influence of diabatically driven circulations interacting with the trough–jet storm system.
- Forecasted daily rainfall by the WRF model simulations in terms of the structure and magnitude of the five ESCSs was closer to the accuracy.
- In the case of ESCS Sidr 2007 and Amphan 2020, the forecast from day 2 onwards showed a lower spatial distribution of the accumulated rainfall forecast due to more significant errors in the track.

  The overall performance of the model forecast was assessed for using skill score metrics, including POD, the Brier Score, and the Critical Success Index. These metrics showed values of 96% for rather heavy rainfall (35.6–64.4 mm/day) and 80% for heavy rainfall (64.5–124.4 mm/day), 0.014 for the Brier Score, and 0.67 for the Critical Success Index. It was concluded that the model performance is good.
- The warm core structure varies from 4 km to 12 km in most of the simulated cases, while in the observation, it varied from 10 km to 14 km.
- The maximum reflectivity of Cyclone Hudhud was well predicted in terms of space and magnitude using the WRF model simulations. In addition, eye, eye size, eyewall, and rain band were well forecasted.

It was concluded in the present study that the simulations of cyclonic parameters, such as track, intensity, rapid intensification, precipitation, and storm structures, performed well with the IMDAA reanalysis datasets during the passage of the majority of ESCSs over the Bay of Bengal region. In addition, this is expected to have several practical implications for forecasting and advancing disaster management strategies in the Bay of Bengal region.

Supplementary Materials: The following supporting information can be downloaded at: https://www.mdpi.com/article/10.3390/cli13010017/s1, Figure S1: Daily accumulated rainfall (in mm/day) from Day-1 to Day-4 valid at 0000 UTC from 18 May to 21 May 2020, simulated (a–d, left panel) and TRMM (e–h, right panel); Figure S2: Daily accumulated rainfall (in mm/day) from Day-1 to Day-4 valid at 0000 UTC from 30 April to 03 May 2019, simulated (a–d, left panel) and TRMM (e–h, right panel); Figure S3: Daily accumulated rainfall (in mm/day) from Day-1 to Day-4 valid at 0000 UTC from 10 October to 13 October 2014, simulated (a–d, left panel) and TRMM (e–h, right panel); Figure S4: Daily accumulated rainfall (in mm/day) from Day-1 to Day-4 valid at 0000 UTC from 10 October to 13 October 2013, simulated (a–d, left panel) and TRMM (e–h, right panel); Figure S5: Daily accumulated rainfall (in mm/day) from Day-1 to Day-4 valid at 0000 UTC from 13 November to 16 November 2007, simulated (a–d, left panel) and TRMM (e–h, right panel).

Author Contributions: Conceptualization, K.S.S.; methodology, T.K. and K.S.S.; software, T.K.; validation, T.K., K.S.S. and S.N.; formal analysis, K.S.S. and T.K.; investigation, T.K., K.S.S. and S.N.; data curation, T.K. and K.S.S.; writing, original draft preparation, T.K., K.S.S. and S.N.; writing, review and editing, K.S.S., T.K. and S.N.; visualization, K.S.S., T.K. and S.N.; supervision, K.S.S. All authors have read and agreed to the published version of the manuscript.

Funding: The authors sincerely acknowledge the financial support by DST-SERB Project file no. ECR/2018/001185.

Data Availability Statement: 1. The India Meteorological Department best-fit track data https://rsmcnewdelhi.imd.gov.in/report.php?internal_menu=MzM=, accessed 14 January 2023. 2. CIRA https://rammb-data.cira.colostate.edu/tc_realtime, accessed on 20 February 2020, with freely available data used for validation. 3. The IMDAA reanalysis datasets are available at the NCMRWF site: https://rds.ncmrwf.gov.in/. 4. TRMM datasets available at: https://giovanni.gsfc.nasa.gov/giovanni.

Acknowledgments: The authors sincerely acknowledge the NCMRWF and IMD for providing the Indian Monsoon Data Assimilation and Analysis (IMDAA) and observed best-fit track datasets, as well as the Doppler Weather Radar (DWR) observations, respectively. Thank you very much to NCAR for providing the WRF software (WRFV4.2) and NASA for the TRMM precipitation datasets. The authors also want to thank the Indian Monsoon Data Assimilation and Analysis (IMDAA) and observed best-fit track datasets, as well as the Doppler Weather Radar (DWR) observations. We acknowledge the ECMWF for providing the ERA-Interim and ERA5 data. Authors thank NOAA, USA, for providing the NCEP FNL data. We are very thankful to Muraganandam R. for his support in plotting using the ArcGIS tools. Thatiparthi K. thanks the Vellore Institute of Technology for providing research facilities and funding. Finally, we appreciate the anonymous reviewer for their constructive comments to improve the quality of the manuscript.

Conflicts of Interest: The authors declare that they have no conflicts of interest. Sridhara Nayak is a contributor and his company has no role in it.

References

1. Srivastava, A.K.; Ray, K.S.; De, U.S. Trends in the frequency of cyclonic disturbances and their intensification over Indian seas. *Mausam* **2000**, *51*, 113–118. [CrossRef]
2. Singh, O.P.; Khan, T.M.A.; Rahman, S. Changes in the frequency of tropical cyclones over the North Indian Ocean. *Meteorol. Atmos. Phys.* **2000**, *75*, 11–20. [CrossRef]
3. Singh, O.P.; Khan, T.M.A.; Rahman, M.S. Has the frequency of intense tropical cyclones increased in the north Indian Ocean? *Curr. Sci.* **2001**, *80*, 575–580.
4. Murakami, H.; Vecchi, G.A.; Underwood, S. Increasing frequency of extremely severe cyclonic storms over the Arabian Sea. *Nat. Clim. Chang.* **2017**, *7*, 885–889. [CrossRef]
5. Singh, K.S.; Albert, J.; Bhaskaran, P.K.; Alam, P. Numerical simulation of an extremely severe cyclonic storm over the Bay of Bengal using WRF modelling system: Influence of model initial condition. *Model. Earth Syst. Environ.* **2021**, *7*, 2741–2752. [CrossRef]
6. Swapna, P.; Sreeraj, P.; Sandeep, N.; Jyoti, J.; Krishnan, R.; Prajeesh, A.G.; Ayantika, D.C.; Manmeet, S. Increasing frequency of extremely severe cyclonic storms in the North Indian Ocean by anthropogenic warming and Southwest monsoon weakening. *Geophys. Res. Lett.* **2022**, *49*, e2021GL094650. [CrossRef]
7. Neumann, B.; Vafeidis, A.T.; Zimmermann, J.; Nicholls, R.J. Future coastal population growth and exposure to sea-level rise and coastal flooding-a global assessment. *PLoS ONE* **2015**, *10*, e0118571. [CrossRef]
8. Hauer, M.E.; Hardy, D.; Kulp, S.A.; Mueller, V.; Wrathall, D.J.; Clark, P.U. Assessing population exposure to coastal flooding due to sea level rise. *Nat. Commun.* **2021**, *12*, 6900. [CrossRef]
9. Sahoo, B.; Bhaskaran, P.K. Assessment on historical cyclone tracks in the Bay of Bengal, east coast of India. *Int. J. Climatol.* **2016**, *36*, 95–109. [CrossRef]
10. Mohapatra, M.; Bandyopadhyay, B.K.; Nayak, D.P. Evaluation of operational tropical cyclone intensity forecasts over north Indian Ocean issued by India Meteorological Department. *Nat. Hazards* **2013**, *68*, 433–451. [CrossRef]
11. Mohapatra, M.; Nayak, D.P.; Sharma, R.P.; Bandyopadhyay, B.K. Evaluation of official tropical cyclone track forecast over north Indian Ocean issued by India Meteorological Department. *J. Earth Syst Sci.* **2013**, *122*, 589–601. [CrossRef]
12. Singh, K.S.; Bhaskaran, P.K. Impact of lateral boundary and initial conditions in the prediction of Bay of Bengal cyclones using WRF model and its 3D-VAR data assimilation system. *J. Atmos. Sol.-Terr. Phys.* **2018**, *175*, 64–75. [CrossRef]
13. Jyoteeshkumar Reddy, P.; Sriram, D.; Gunthe, S.S.; Balaji, C. Impact of climate change on intense Bay of Bengal tropical cyclones of the post-monsoon season: A pseudo global warming approach. *Clim. Dyn.* **2021**, *56*, 2855–2879. [CrossRef]
14. Nayak, S.; Takemi, T. Robust responses of typhoon hazards in northern Japan to global warming climate: Cases of landfalling typhoons in 2016. *Meteorol. Appl.* **2020**, *27*, e1954. [CrossRef]
15. Nayak, S.; Takemi, T. Dynamical Downscaling of Typhoon Lionrock (2016) for Assessing the Resulting Hazards under Global Warming. *J. Meteorol. Soc. Jpn* **2019**, *97*, 123–143. [CrossRef]
16. Singh, K.S.; Nayak, S.; Maity, S.; Nayak, H.P.; Dutta, S. Prediction of extremely severe cyclonic storm "Fani" using moving nested domain. *Atmosphere* **2023**, *14*, 637. [CrossRef]
17. Nayak, S.; Takemi, T. Quantitative estimations of hazards resulting from Typhoon Chanthu (2016) for assessing the impact in current and future climate. *Hydrol. Res. Lett.* **2019**, *13*, 20–27. [CrossRef]
18. Xiao, Q.; Kuo, Y.H.; Zhang, Y.; Barker, D.M.; Won, D.J. A tropical cyclone bogus data assimilation scheme in the MM5 3D-Var system and numerical experiments with Typhoon Rusa (2002) near landfall. *J. Meteorol. Soc. Jpn.* **2006**, *84*, 671–689. [CrossRef]
19. Elsberry, R.L.; Tsai, H.C.; Chin, W.C.; Marchok, T.P. Advanced global model ensemble forecasts of tropical cyclone formation, and intensity predictions along medium-range tracks. *Atmosphere* **2020**, *11*, 1002. [CrossRef]

20. Srivastava, A.; Prasad, V.S.; Das, A.K.; Sharma, A. A HWRF-POM-TC coupled model forecast performance over North Indian Ocean: VSCS TITLI & VSCS LUBAN. *Trop. Cyclone Res. Rev.* **2021**, *10*, 54–70.
21. Bachmann, K.; Torn, R.D. Validation of HWRF-based probabilistic TC wind and precipitation forecasts. *Weather Forecast.* **2021**, *36*, 2057–2070. [CrossRef]
22. Singh, K.S.; Thankachan, A.; Thatiparthi, K.; Reshma, M.S.; Albert, J.; Bonthu, S.; Bhaskaran, P.K. Prediction of rapid intensification for land-falling extremely severe cyclonic storms in the Bay of Bengal. *Theor. Appl. Climatol.* **2022**, *147*, 1359–1377. [CrossRef]
23. Nolan, D.S.; Zhang, J.A.; Stern, D.P. Evaluation of planetary boundary layer parameterizations in tropical cyclones by comparison of in situ observations and high-resolution simulations of Hurricane Isabel (2003). Part I: Initialization, maximum winds, and the outer-core boundary layer. *Mon. Weather. Rev.* **2009**, *137*, 3651–3674. [CrossRef]
24. Singh, K.S.; Mandal, M. Sensitivity of mesoscale simulation of Aila Cyclone to the parameterization of physical processes using WRF Model. In *Monitoring and Prediction of Tropical Cyclones in the Indian Ocean and Climate Change*; Springer: Dordrecht, The Netherlands, 2014; pp. 300–308.
25. Singh, K.S.; Bhaskaran, P.K. Impact of PBL and convection parameterization schemes for prediction of severe land-falling Bay of Bengal cyclones using WRF-ARW model. *J. Atmos. Sol.-Terr. Phys.* **2017**, *165*, 10–24. [CrossRef]
26. Zhang, J.A.; Kalina, E.A.; Biswas, M.K.; Rogers, R.F.; Zhu, P.; Marks, F.D. A review and evaluation of planetary boundary layer parameterizations in hurricane weather research and forecasting model using idealized simulations and observations. *Atmosphere* **2020**, *11*, 1091. [CrossRef]
27. Park, J.; Cha, D.H.; Lee, M.K.; Moon, J.; Hahm, S.J.; Noh, K.; Chan, J.C.L.; Bell, M. Impact of cloud microphysics schemes on tropical cyclone forecast over the western North Pacific. *J. Geophys. Res. Atmos.* **2020**, *125*, e2019JD032288. [CrossRef]
28. Wu, D.; Zhang, F.; Chen, X.; Ryzhkov, A.; Zhao, K.; Kumjian, M.R.; Chen, X.; Chan, P.W. Evaluation of microphysics schemes in tropical cyclones using polarimetric radar observations: Convective precipitation in an outer rainband. *Mon. Weather. Rev.* **2021**, *149*, 1055–1068. [CrossRef]
29. Rakesh, V.; Singh, R.; Pal, P.K.; Joshi, P.C. Impact of satellite soundings on the simulation of heavy rainfall associated with tropical depressions. *Nat. Hazards.* **2011**, *58*, 945–980. [CrossRef]
30. Zhao, Y.; Wang, B.; Liu, J. A DRP–4DVar data assimilation scheme for typhoon initialization using sea level pressure data. *Mon. Weather. Rev.* **2012**, *140*, 1191–1203. [CrossRef]
31. Srinivas, C.V.; Bhaskar Rao, D.; Yesubabu, V.; Baskaran, R.; Venkatraman, B. Tropical cyclone predictions over the Bay of Bengal using the high-resolution Advanced ResearchWeather Research and Forecasting (ARW) model. *Q. J. R. Meteorol. Soc.* **2013**, *139*, 1810–1825. [CrossRef]
32. Yesubabu, V.; Srinivas, C.V.; Hariprasad, K.B.R.R.; Baskaran, R. A study on the impact of observation assimilation on the numerical simulation of tropical cyclones JAL and THANE using 3DVAR. *Pure Appl. Geophys.* **2014**, *171*, 2023–2042. [CrossRef]
33. Osuri, K.K.; Mohanty, U.C.; Routray, A.; Niyogi, D. Improved prediction of Bay of Bengal tropical cyclones through assimilation of Doppler weather radar observations. *Mon. Weather. Rev.* **2015**, *143*, 4533–4560. [CrossRef]
34. Greeshma, M.M.; Srinivas, C.V.; Yesubabu, V.; Naidu, C.V.; Baskaran, R.; Venkatraman, B. Impact of local data assimilation on tropical cyclone predictions over the Bay of Bengal using the ARW model. *Ann. Geophys.* **2015**, *33*, 805–828. [CrossRef]
35. Routray, A.; Mohanty, U.C.; Osuri, K.K.; Kar, S.C.; Niyogi, D. Impact of satellite radiance data on simulations of Bay of Bengal tropical cyclones using the WRF-3DVAR modeling system. *IEEE Trans. Geosci. Remote Sens.* **2016**, *54*, 2285–2303. [CrossRef]
36. Singh, K.S.; Mandal, M.; Bhaskaran, P.K. Impact of radiance data assimilation on the prediction performance of cyclonic storm SIDR using WRF-3DVAR modelling system. *Meteorol. Atmos. Phys.* **2019**, *131*, 11–28. [CrossRef]
37. Elsberry, R.L.; Feldmeier, J.W.; Chen, H.J.; Peng, M.; Velden, C.S.; Wang, Q. Challenges and Opportunities with New Generation Geostationary Meteorological Satellite Datasets for Analyses and Initial Conditions for Forecasting Hurricane Irma (2017) Rapid Intensification Event. *Atmosphere* **2020**, *11*, 1200. [CrossRef]
38. Zhang, S.; Pu, Z. Evaluation of the four-dimensional ensemble-variational hybrid data assimilation with self-consistent regional background error covariance for improved hurricane intensity forecasts. *Atmosphere* **2020**, *11*, 1007. [CrossRef]
39. Zhang, J.; Feng, J.; Li, H.; Zhu, Y.; Zhi, X.; Zhang, F. Unified ensemble mean forecasting of tropical cyclones based on the feature-oriented mean method. *Weather Forecast.* **2021**, *36*, 1945–1959. [CrossRef]
40. Chen, X.; Xue, M.; Fang, J. Rapid intensification of Typhoon Mujigae (2015) under different sea surface temperatures: Structural changes leading to rapid intensification. *J. Atmos. Sci.* **2018**, *75*, 4313–4335. [CrossRef]
41. Liao, X.; Li, T.; Ma, C. Moist Static Energy and Secondary Circulation Evolution Characteristics during the Rapid Intensification of Super Typhoon Yutu (2007). *Atmosphere* **2022**, *13*, 1105. [CrossRef]
42. Wu, Z.; Zhang, Y.; Zhang, L.; Zheng, H. Improving the WRF Forecast of Landfalling Tropical Cyclones Over the Asia-Pacific Region by Constraining the Cloud Microphysics Model with GPM Observations. *Geophys. Res. Lett.* **2022**, *49*, e2022GL100053. [CrossRef]
43. DeMaria, M.; Sampson, C.R.; Knaff, J.A.; Musgrave, K.D. Is tropical cyclone intensity guidance improving? *Bull. Am. Meteorol. Soc.* **2014**, *95*, 387–398. [CrossRef]

44. Feng, J.; Wang, X. Impact of increasing horizontal and vertical resolution during the HWRF hybrid EnVar data assimilation on the analysis and prediction of Hurricane Patricia (2015). *Mon. Weather. Rev.* **2021**, *149*, 419–441. [CrossRef]
45. Nayak, S.; Takemi, T. Structural characteristics of typhoons Jebi (2018), Faxai (2019), and Hagibis (2019). *Meteorol. Atmos. Phys.* **2023**, *135*, 34. [CrossRef]
46. Nayak, S.; Takemi, T. Typhoon-induced precipitation characterization over northern Japan: A case study for typhoons in 2016. *Prog. Earth Planet. Sci.* **2020**, *7*, 39. [CrossRef]
47. Zhang, X.; Quirino, T.; Yeh, K.S.; Gopalakrishnan, S.; Marks, F.; Goldenberg, S.; Aberson, S. HWRFx: Improving hurricane forecasts with high-resolution modeling. *Comput. Sci. Eng.* **2010**, *13*, 13–21. [CrossRef]
48. Gopalakrishnan, S.G.; Goldenberg, S.; Quirino, T.; Zhang, X.; Marks, F.; Yeh, K.S.; Atlas, R.; Tallapragada, V. Toward improving high-resolution numerical hurricane forecasting: Influence of model horizontal grid resolution, initialization, and physics. *Weather Forecast.* **2012**, *27*, 647–666. [CrossRef]
49. Hodges, K.; Cobb, A.; Vidale, P.L. How well are tropical cyclones represented in reanalysis datasets? *J. Clim.* **2017**, *30*, 5243–5264. [CrossRef]
50. Lee, R.; Chen, L.; Ren, G. A comparison of East-Asia landfall tropical cyclone in recent reanalysis datasets--before and after satellite era. *Front. Earth Sci.* **2023**, *10*, 1026945. [CrossRef]
51. Routray, A.; Dutta, D.; Desamsetti, S.; Patel, S.S.; George, J.P.; Prasad, V.S. Study pre-and post-monsoon storms over NIO region using high resolution IMDAA reanalysis dataset. *Clim. Dyn.* **2024**, *62*, 555–574. [CrossRef]
52. Malakar, P.; Kesarkar, A.P.; Bhate, J.N.; Singh, V.; Deshamukhya, A. Comparison of reanalysis data sets to comprehend the evolution of tropical cyclones over North Indian Ocean. *Earth Space Sci.* **2020**, *7*, e2019EA000978. [CrossRef]
53. Skamarock, W.C.; Klemp, J.B.; Dudhia, J.; Gill, D.O.; Liu, Z.; Berner, J.; Wang, W.; Powers, J.G.; Duda, M.G.; Barker, D.M.; et al. *A Description of the Advanced Research WRF Model Version 4*; National Center for Atmospheric Research: Boulder, CO, USA, 2019; Volume 145, p. 550.
54. Shikhovtsev, A.Y.; Kovadlo, P.G.; Kopylov, E.A.; Ibrahimov, M.A.; Ehgamberdiev, S.A.; Tillayev, Y.A. Energy Spectra of Atmospheric Turbulence for Calculating 2*n* Parameter. I. Maidanak and Suffa Observatories in Uzbekistan. *Atmosphere* **2021**, *12*, 1614. [CrossRef]
55. European Centre for Medium-Range Weather Forecasts. Greater Atmospheric Resolution Improves the Prediction of Tropical Cyclones. ECMWF. 2022. Available online: https://www.ecmwf.int/en/newsletter/172/news/greater-atmospheric-resolution-improves-prediction-tropical-cyclones (accessed on 10 July 2022).
56. Mandal, M.; Mohanty, U.C.; Potty, K.; Sarkar, A. Impact of horizontal resolution on prediction of tropical cyclones over Bay of Bengal using a regional weather prediction model. *J. Earth. Syst. Sci.* **2003**, *112*, 79–93. [CrossRef]
57. Bhaskar Rao, D.V.; Hari Prasad, D.; Srinivas, D. Impact of horizontal resolution and the advantages of the nested domains approach in the prediction of tropical cyclone intensification and movement. *J. Geophys. Res Atmos.* **2009**, *114*, D11. [CrossRef]
58. Chutia, L.; Pathak, B.; Parottil, A.; Bhuyan, P.K. Impact of microphysics parameterizations and horizontal resolutions on simulation of "MORA" tropical cyclone over Bay of Bengal using Numerical Weather Prediction Model. *Meteorol Atmos Phys.* **2019**, *131*, 1483–1495. [CrossRef]
59. Osuri, K.K.; Mohanty, U.C.; Routray, A.; Kulkarni, M.A.; Mohapatra, M. Customization of WRF-ARW model with physical parameterization schemes for the simulation of tropical cyclones over North Indian Ocean. *Nat. Hazards* **2012**, *63*, 1337–1359. [CrossRef]
60. Osuri, K.K.; Mohanty, U.C.; Routray, A.; Mohapatra, M.; Niyogi, D. Real-time track prediction of tropical cyclones over the North Indian Ocean using the ARW model. *J. Appl. Meteorol. Climatol.* **2013**, *52*, 2476–2492. [CrossRef]
61. Nellipudi, N.R.; Viswanadhapalli, Y.; Challa, V.S.; Vissa, N.K.; Langodan, S. Impact of surface roughness parameterizations on tropical cyclone simulations over the Bay of Bengal using WRF-OML model. *Atmos. Res.* **2021**, *262*, 105779. [CrossRef]
62. Lin, Y.L.; Farley, R.D.; Orville, H.D. Bulk parameterization of the snow field in a cloud model. *J. Appl. Meteorol. Climatol.* **1983**, *22*, 1065–1092. [CrossRef]
63. Chen, S.H.; Sun, W.Y. A one-dimensional time dependent cloud model. *J. Meteorol. Soc. Jpn.* **2002**, *80*, 99–118. [CrossRef]
64. Kain, J.S. The Kain–Fritsch convective parameterization: An update. *J. Appl. Meteorol.* **2004**, *43*, 170–181. [CrossRef]
65. Hong, S.Y.; Noh, Y.; Dudhia, J. A new vertical diffusion package with an explicit treatment of entrainment processes. *Mon. Weather. Rev.* **2006**, *134*, 2318–2341. [CrossRef]
66. Mlawer, E.J.; Taubman, S.J.; Brown, P.D.; Iacono, M.J.; Clough, S.A. Radiative transfer for inhomogeneous atmospheres: RRTM, a validated correlated-k model for the longwave. *J. Geophys. Res. Atmos.* **1997**, *102*, 16663–16682. [CrossRef]
67. Dudhia, J. Numerical study of convection observed during the winter monsoon experiment using a mesoscale two-dimensional model. *J. Atmos. Sci.* **1989**, *46*, 3077–3107. [CrossRef]
68. Niu, G.Y.; Yang, Z.L.; Mitchell, K.E.; Chen, F.; Ek, M.B.; Barlage, M.; Kumar, A.; Manning, K.; Niyogi, D.; Rosero, E.; et al. The community Noah land surface model with multi parameterization options (Noah-MP): 1. Model description and evaluation with local-scale measurements. *J. Geophys. Res. Atmos.* **2011**, *116*, D12109. [CrossRef]
69. Mahmood, S.; Davie, J.; Jermey, P.; Renshaw, R.; George, J.P.; Rajagopal, E.N.; Rani, S.I. Indian monsoon data assimilation and analysis regional reanalysis: Configuration and performance. *Atmos. Sci. Lett.* **2018**, *19*, e808. [CrossRef]

70. Ashrit, R.; Indira Rani, S.; Kumar, S.; Karunasagar, S.; Arulalan, T.; Francis, T.; Routraay, A.; Laskar, S.I.; Mahmood, S.; Jermey, P.; et al. IMDAA regional reanalysis: Performance evaluation during Indian summer monsoon season. *J. Geophys. Res. Atmos.* **2020**, *125*, e2019JD030973. [CrossRef]
71. Rani, S.I.; Arulalan, T.; George, J.P.; Rajagopal, E.N.; Renshaw, R.; Maycock, A.; Barker, D.M.; Rajeevan, M. IMDAA: High-resolution satellite-era reanalysis for the Indian monsoon region. *J. Clim.* **2021**, *34*, 5109–5133. [CrossRef]
72. Demuth, J.L.; De Maria, M.; Knaff, J.A.; Haar, T.H.V. Evaluation of Advanced Microwave Sounding Unit tropical-cyclone intensity and size estimation algorithms. *J. Appl. Meteorol. Climatol.* **2004**, *43*, 282–296. [CrossRef]
73. Mohapatra, M.; Bandyopadhyay, B.K.; Tyagi, A. Best track parameters of tropical cyclones over the North Indian Ocean: A review. *Nat. Hazards.* **2012**, *63*, 1285–1317. [CrossRef]
74. Albert, J.; Bhaskaran, P.K. Evaluation of track length, residence time and translational speed for tropical cyclones in the North Indian Ocean. *ISH J. Hydraul. Eng.* **2020**, *28*, 34–41. [CrossRef]
75. Reshma, M.S.; Singh, K.S. Role of PBL and air-sea flux parameterization schemes in the forecast of super cyclone Amphan and ESCS Phailin in the cloud-resolving scale using WRF-ARW model. *Model. Earth Syst. Environ.* **2024**, *10*, 5449–5467. [CrossRef]
76. Baki, H.; Balaji, C.; Srinivasan, B. Impact of data assimilation on a calibrated WRF model for the prediction of tropical cyclones over the Bay of Bengal. *Curr. Sci.* **2022**, *122*, 569–583. [CrossRef]
77. Chanchal, K.; Singh, K.S. Role of high-resolution modeling system in prediction of heavy rainfall events over Tamil Nadu and Kerala on different global/regional datasets. *Model. Earth Syst. Environ.* **2024**, *10*, 3827–3843. [CrossRef]
78. Dube, A.; Ashrit, R.; Kumar, S.; Mamgain, A. Improvements in tropical cyclone forecasting through ensemble prediction system at NCMRWF in India. *Trop. Cyclone Res. Rev.* **2020**, *9*, 106–111. [CrossRef]
79. Kotal, S.D.; Bhattacharya, S.K.; Bhowmik, S.R. Development of NWP based objective cyclone prediction system (CPS) for North Indian Ocean tropical cyclones—Evaluation of performance. *Trop. Cyclone Res. Rev.* **2014**, *3*, 162–177.
80. Klotzbach, P.J.; Wood, K.M.; Schreck III, C.J.; Bowen, S.G.; Patricola, C.M.; Bell, M.M. Trends in global tropical cyclone activity: 1990–2021. *Geophys. Res. Lett.* **2022**, *49*, e2021GL095774. [CrossRef]
81. Vemuri, A.; Buckingham, S.; Munters, W.; Helsen, J.; Van Beeck, J. Sensitivity analysis of mesoscale simulations to physics parameterizations over the Belgian North Sea using Weather Research and Forecasting–Advanced Research WRF (WRF-ARW). *Wind Energy Sci.* **2022**, *7*, 1869–1888. [CrossRef]